SANDIA REPORT SAND83-8214 • Unlimited Release • UC-25
Printed May 1983

Slow Strain Rate Testing of 2.25Cr-1Mo in Molten Nitrate Salt

S. H. Goods

Prepared by
Sandia National Laboratories
Albuquerque, New Mexico 87185 and Livermore, California 94550
for the United States Department of Energy
under Contract DE-AC04-76DP00789

SF 2900-Q(6-82)

Issued by Sandia National Laboratories, operated for the United States Department of Energy by Sandia Corporation.

SAND83-8214
Unlimited Release
Printed May 1983

UC-25

SLOW STRAIN RATE TESTING OF 2.25Cr-1Mo IN MOLTEN NITRATE SALT

S. H. Goods
Materials Science Division
Sandia National Laboratories, Livermore

ABSTRACT

The influence of an oxidizing molten nitrate salt (60% $NaNO_3$-40% KNO_3) on the mechanical properties of 2.25Cr-1Mo has been examined through a series of slow strain rate tests at 450°C and 525°C. By comparing fracture strain, reduction in area and the ultimate strength of air exposed specimens to these same parameters for specimens tested in the binary salt mixture, the susceptibility of the alloy to environmental degradation could be ascertained.

Exposure to the nitrate resulted in a loss of ductility as measured by either the engineering fracture strain or reduction in area at both temperatures studied. At these temperatures, the ductility loss was most pronounced at the lowest strain rates ($1x10^{-7}sec^{-1}$). In general, for all strain rates examined, the degree of ductility loss was greater at 525°C than at 450°C.

Metallographic observations revealed that severe surface oxidation occurred as the result of exposure to the molten salt. These surface scales were found to be non-adherent and easily spalled. The rapid formation of these corrosion products and the inability of the material to form a protective barrier against further oxidation is consistent with the ductility loss observed in the salt-exposed specimens.

CONTENTS

ILLUSTRATIONS

TABLES

SLOW STRAIN RATE TESTING OF 2.25Cr-1Mo IN MOLTEN NITRATE SALT

Introduction

2.25Cr-1Mo has been proposed for use as a high temperature fluid containment material in advanced solar central receivers (SCR). These proposed designs call for the use of a condensed phase fluid as either the coolant (heat transport fluid) or as the sensible heat storage medium. The choice of this fluid is largely one of economics based upon a combination of factors including cost and optimal thermophysical characteristics. For current receiver designs, this choice has been narrowed to the nitrate based salts. Within an SCR, the containment alloy could be used in the construction of a variety of components which would be required to withstand continuous exposure to the salt at peak temperatures on the order of 400-500°C (i.e., low temperature thermal storage or evaporator assemblies). While nitrate salts have been used for some time at these temperatures in a variety of applications including heat transfer and metal heat treating applications, they are generally contained in austenitic stainless steel crucibles (1). There are, therefore, a number of questions regarding the compatibility of a lower alloy material, such as 2.25Cr-1Mo, in these molten nitrate salt environments.

This report details the results of an experimental program in which the effect of long-term salt exposure on the mechanical properties of 2.25Cr-1Mo has been evaluated through a series of slow strain rate tests (SSRT). These tests consist of the application of a constant extension rate imposed on a tensile specimen which has a uniform cross-section exposed to the environment of interest. The behavior of the specimens in salt is compared to the behavior of specimens exposed to an inert or reference environment (in the present case, air) under identical conditions of strain rate and temperature. Fracture strain, reduction in area (RA), and ultimate tensile strength (UTS) are measured as parameters which determine the susceptibility of an alloy to environmental degradation. The test is a versatile method for both the detection of the presence of an environmental embrittlement or stress corrosion cracking phenomenon as well as for analysis of the critical variables which may contribute to the observed material degradation. The variables which may be screened include temperature, strain rate, the particular nitrate salt chemistry or impurity content and the metallurgical condition of the alloy under investigation.

Previous studies have shown that both austenitic and ferritic stainless steels suffer uniform surface attack when immersed in these nitrate salts for extended periods of time (2-4). In order to examine the effect of continuous deformation on the corrosion characteristics of materials in these salts, therefore, it is necessary to perform the mechanical testing at rates slow enough to allow the corrosive environment

to act upon the test alloy before purely mechanical failure occurs. Figure 1 schematically illustrates the expected strain rate dependence of the ductility for a material which suffers from an environmentally induced loss of ductility. In Region I the strain rate is rapid and the resulting test time is short so that a specimen can deform and fracture before the environment can induce a measureable effect. Fracture therefore occurs by the normal process of ductile rupture. In Region II environmentally induced embrittlement occurs and the loss of ductility can be due to any of several factors. Continuous deformation may result in a porous or cracked oxide scale and thus allow for an increased rate of corrosion. When coupled to the imposed deformation, buildup of stresses within the surface scale as it forms can induce or accelerate a spalling or flaking-off process, and expose fresh base metal. This would tend to increase the overall rate of oxide formation and increase the rate of metal loss. Alternatively, deformation-induced cracking of near-surface grain boundaries can allow the aggressive environment to penetrate to regions deep within the specimen. The concomitant loss of load bearing cross-sectional area may result in the earlier onset of necking and fracture. In the extreme case, grain boundary brittle fracture will occur due to attack of the environment on the specimen.

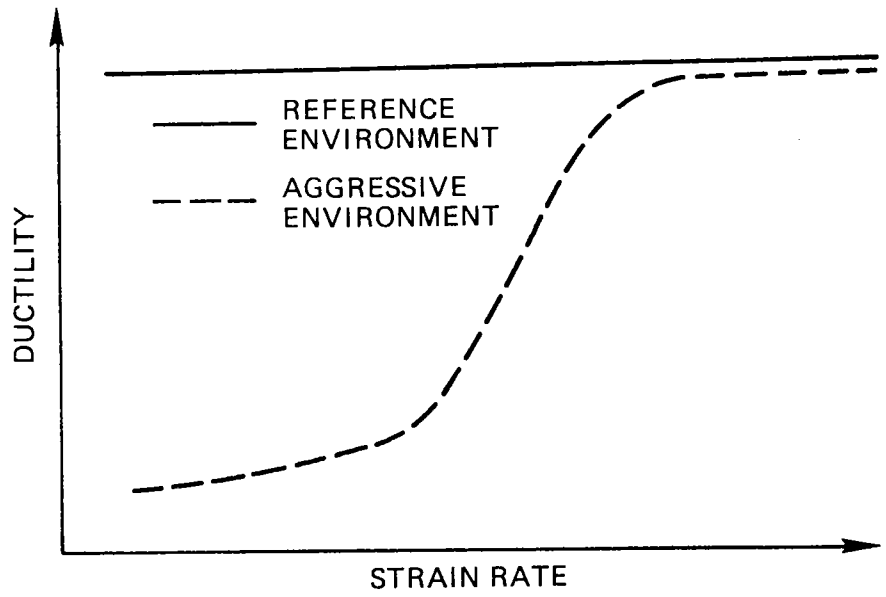

Figure 1. Schematic representation of the effect of strain rate on material ductility as measured in a SSRT experiment for a material which suffers from environmentally induced embrittlement.

Experimental Procedure

Tensile tests were performed at 450°C and 525°C on a 2.25Cr-1Mo alloy with the composition as shown in Table 1. Sheet

TABLE 1

Composition of 2.25Cr-1Mo Alloy (wt%)

Cr	Mo	C	Mn	Si	Cu	Fe
2.31	1.01	0.15	0.57	0.41	0.11	Bal.

tensile specimens were machined from the stock using EDM techniques. The gage length of the specimens was 25.4 mm while the specimen cross-section measured 1.27 mm x 6.35 mm. Prior to machining, the stock was heat treated according to the following schedule:

> Austenitize at 927°C for 1 hour, slow cool to 704°C (1.5°C/min) then hold at 704°C for 2 hours and then cool to room temperature at 6°C/min.

The SSRT test facility consists of two identical load frames with an 18 KN maximum load rating. The frames are geared to allow uniform extension rates of from 2.54×10^{-8} mm/sec to 2.54×10^{-4} mm/sec. Initial strain rates were computed on the basis of the specimen gage length and the chosen extension rate. The particular salt composition was a commercially available 60% $NaNO_3$ - 40% KNO_3 mixture. To contain the molten salt, a 316 stainless steel salt pot with a water cooled collar was placed in the furnace cavity. The furnace was a wide bore crucible type. Specimens were fixtured in a rigid four-column cage suspended from the crosshead and the furnace body containing the salt pot was then raised up around the specimen. Salt temperature was controlled and monitored using type K thermocouples positioned along the specimen gage length. Using a Eurotherm temperature controller and power supply, temperature could be maintained to within $\pm$ 0.5°C of set point. Load vs. time data were recorded continuously on a low speed strip-chart recorder.

After tensile testing, specimens were metallographically prepared and examined using optical microscopy and electron-optical methods. Fracture surfaces were examined using scanning electron microscopy (SEM). Surface oxide chemistry was analyzed in an electron microprobe using energy dispersive x-ray spectroscopy (EDS).

Results and Discussion

Mechanical Properties - 450°C

Figure 2 shows the stress-strain curves generated for the alloy tested in air at 450°C and at the strain rates indicated. The curves reveal that the ultimate strength of the alloy is somewhat rate sensitive, increasing by approximately 60 MPa over the two orders of magnitude increase in initial strain rate. These tests also reveal that the engineering fracture strain tends to decrease slightly with increasing strain rate.

Figure 3 shows the stress-strain curves generated for the alloy tested in salt at 450°C at the same strain rates as in Figure 2. Except for the specimen tested at the lowest strain rate, there is less variation in ultimate strength for these specimens than for those shown in the previous figure. Additionally, specimens tested in salt exhibited a greater UTS than those tested in air. An example of this is shown in Figure 4a which directly compares the stress-strain curves for salt and air exposed specimens tested at an initial strain rate 1 x $10^{-7}sec^{-1}$. This behavior was observed at all strain rates tested as illustrated by Appendix Figure [1].

It is difficult to rationalize this environmentally induced increase in strength for this alloy. Dohle et al. (5) have discussed this type of phenomena in general and indicate that an increase in high temperature strength may occur by the precipitation of oxide corrosion products in a material. This, they reason, may lead to a decrease in grain boundary sliding (if precipitation occurs intergranularly) or to precipitate strengthening (if precipitation occurs homogenously). However, in the present case, detailed metallographic observations do not reveal the presence of any environmentally induced "internal" oxidation. Alternatively, they suggest that alloys which develop surface scales as a corrosion product may act as a composite. If the strength of the surface scale is high, the overall material strength will increase. Figure 4b, however, shows that this strengthening occurred even for the highest strain rates studied ($10^{-5}sec^{-1}$) where, as will be shown, the degree of salt and air induced surface corrosion was comparable. Since these surface scales were of similar thickness it seems unlikely that they can result in an increased strength for the salt exposed specimen over that determined for an air exposed specimen. It will also be shown that the scales which do form spall easily and do not adhere well to the alloy. It is hard then to justify the observed strengthening according to the latter argument.

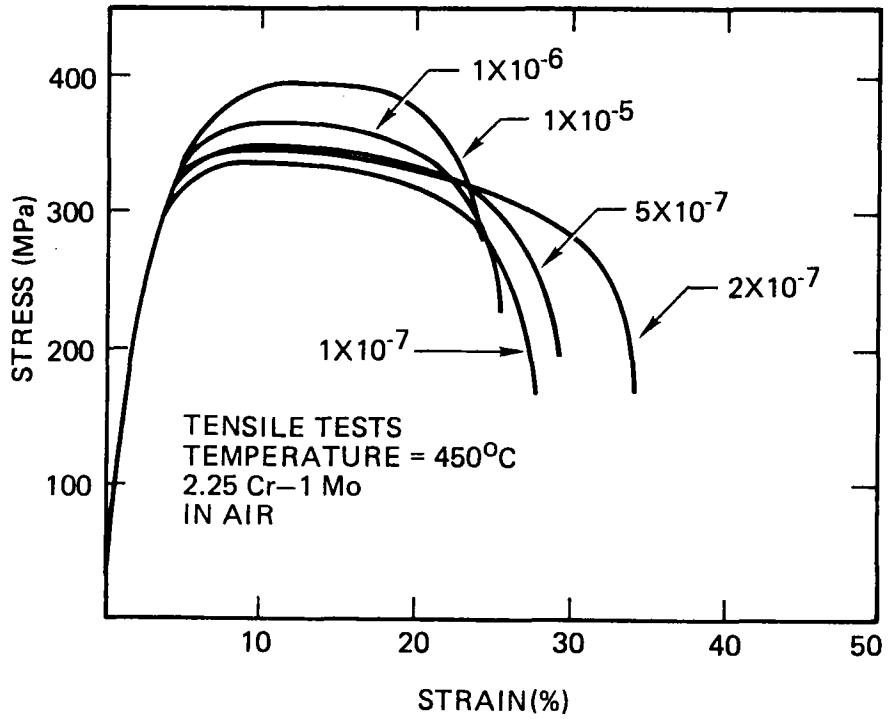

Figure 2. Stress-strain curves for 2.25Cr-2Mo tested at 450°C in air. Strain rates indicated are in sec^{-1}.

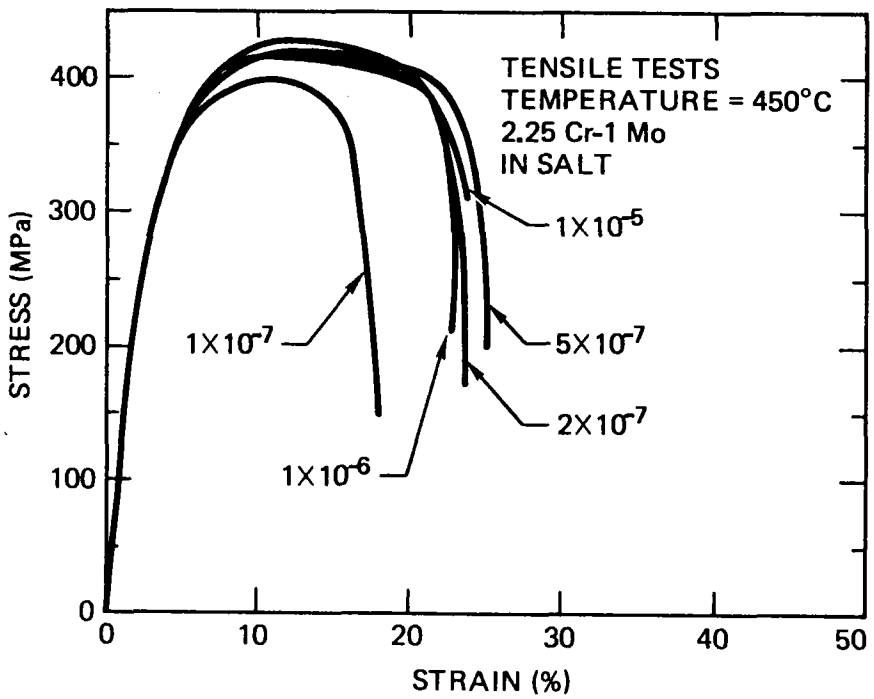

Figure 3. Stress-strain curves for 2.25Cr-1Mo tested at 450°C in molten nitrate salt. Strain rates indicated are in sec^{-1}.

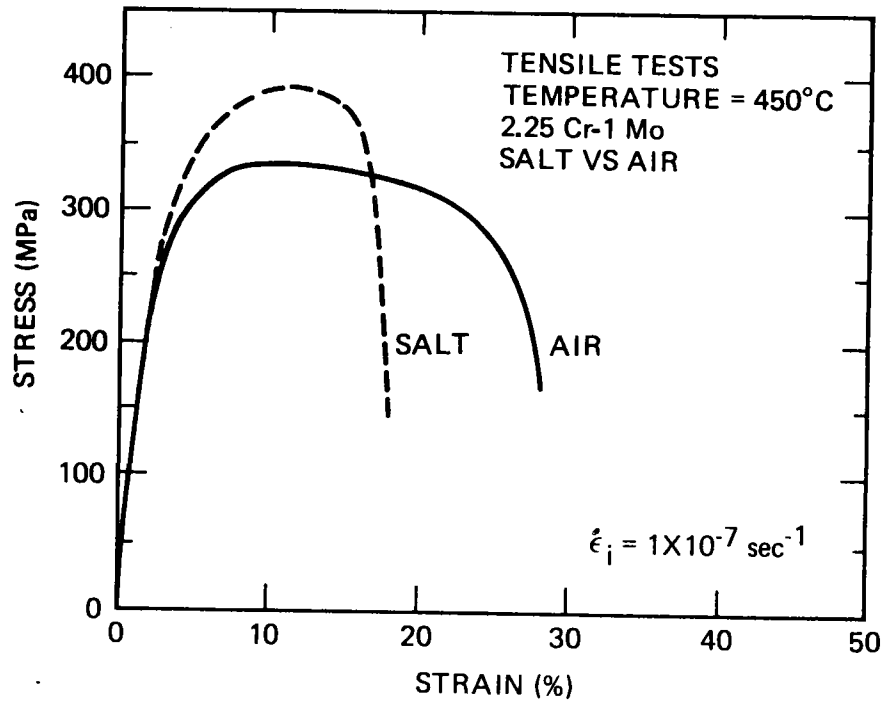

a)

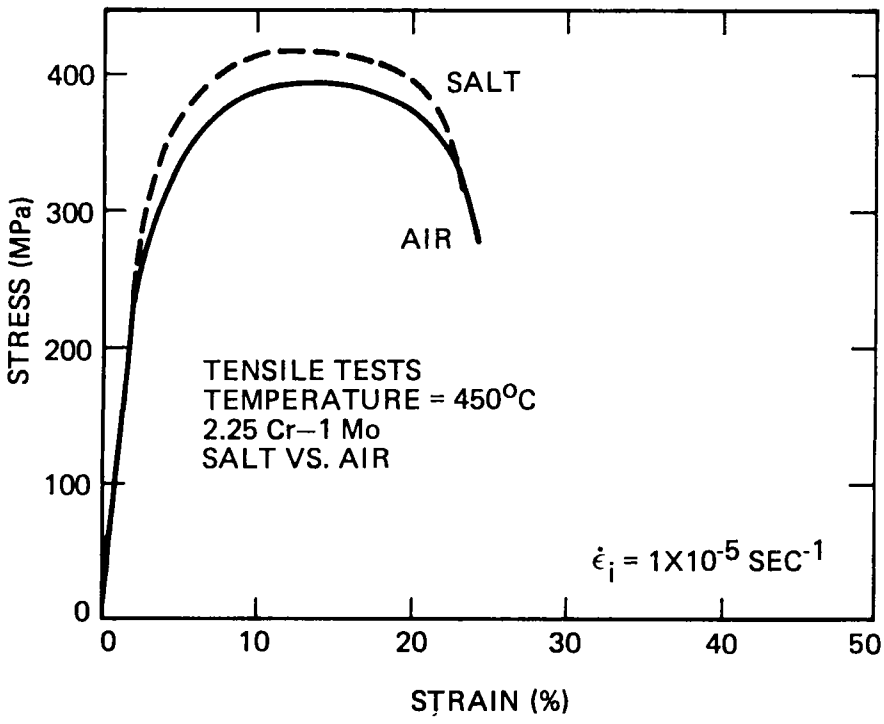

b)

Figure 4. a) Comparison of the tensile behavior of the alloy in salt vs. air at 450°C ($\dot{\varepsilon} = 1 \times 10^{-7}$ sec^{-1}).

b) Comparison of the tensile behavior of the alloy in salt vs. air at 450°C ($\dot{\varepsilon} = 1 \times 10^{-5}$sec^{-1})

The data for all the mechanical testing is summarized in Table 2. From this table it can be seen that there was a progressive degradation

TABLE 2

Tensile Properties of 2.25Cr-1Mo at 450°C

Strain Rate (sec^{-1})	Environment	UTS (MPa)	Elongation (%)	RA (%)
1×10^{-5}	Air	398	22.9	70.3
	Salt	421	21.0	63.2
1×10^{-6}	Air	367	25.9	78.5
	Salt	425	23.0	56.5
5×10^{-7}	Air	348	29.8	79.3
	Salt	418	25.2	55.0
2×10^{-7}	Air	344	34.6	78.8
	Salt	421	24.9	51.0
1×10^{-7}	Air	330	28.3	79.2
	Salt	390	18.3	54.1

in ductility with decreasing strain rate (i.e., increasing salt exposure time). Figure 4 also illustrates the ductility loss exhibited by the salt exposed specimens as measured by the strain to fracture. This result is more clearly displayed in Figure 5, which shows the influence of initial strain rate on total elongation (Fig. 5a) and reduction in area (Fig. 5b). At high strain rates, the ductility of the alloy was essentially unaffected by environment as measured by the engineering fracture strain. At the lowest strain rates and therefore the longest salt exposure time, engineering fracture strain was significantly reduced. Reduction in area appears to be a more sensitive measure of environmental susceptibility being measurably lower for the salt exposed specimens at all strain rates tested. Figure 6 shows the fracture surfaces for the specimens tested in salt and in air at both the highest and lowest strain rates. While they do not reveal any obvious environmentally induced fracture mode change, they do indicate that in all cases fracture was transgranular. At the lowest strain rates, however, the fracture surfaces appear quite featureless.

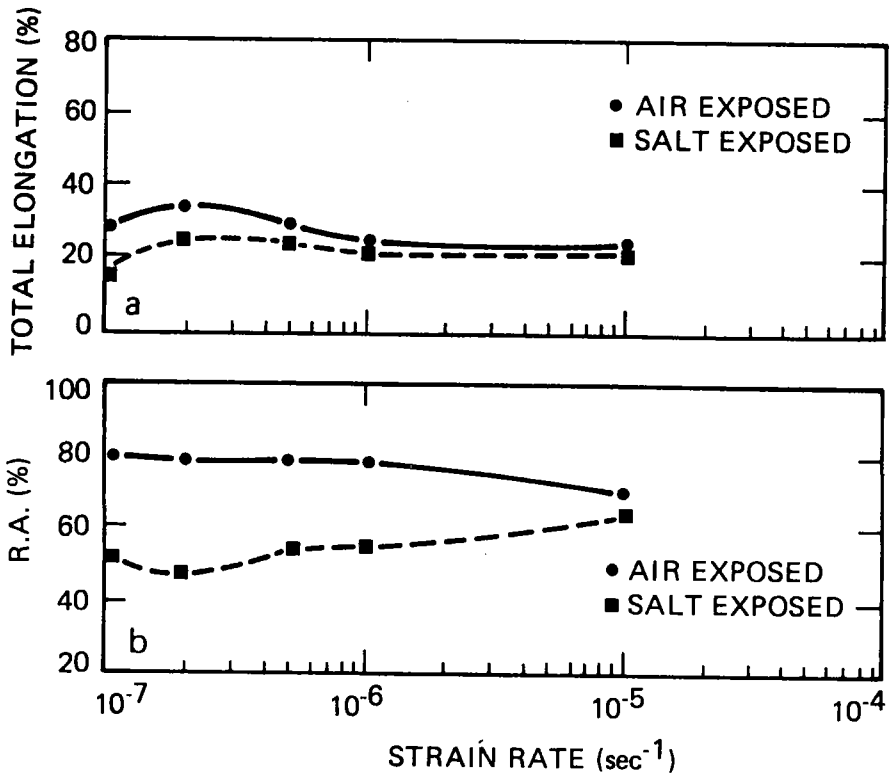

Figure 5. a) Effect of strain rate on total elongation (fracture strain) for 2.25Cr-1Mo at 450°C.

b) Effect of strain rate on reduction in area (R.A.) at 450°C.

Oxide Structure - 450°C

2.25Cr-1Mo oxidizes at 450°C when exposed to either air or the nitrate salt environments. The surfaces scales formed by exposure of the alloy to either environment were generally non-adherent. Because of the extensive oxide spallation which occurred during post-test handling of the specimens and during metallographic preparation, quantitative analyses of the kinetics of oxidation and scale formation were not possible. Figures 7 and 8 compare the surface scales formed on undeformed grip sections of specimens tested in salt and air. In each micrograph "a" is from the specimen tested at the slowest initial strain rate while micrograph "e" is from the specimen tested at the fastest strain rate. The times associated with each micrograph refer to the total test time and therefore very nearly approximate the total environmental exposure time. In most cases it can be seen that the surface scales shown in either figure have separated from the base metal. Figure 7a, d and e show clear evidence of spallation and blistering. The oxides formed on the salt exposed surfaces were generally thicker than those formed on the air exposed surfaces; however, their separation due to poor adhesion precluded any detailed comparison between the oxidation kinetics in salt vs. air.

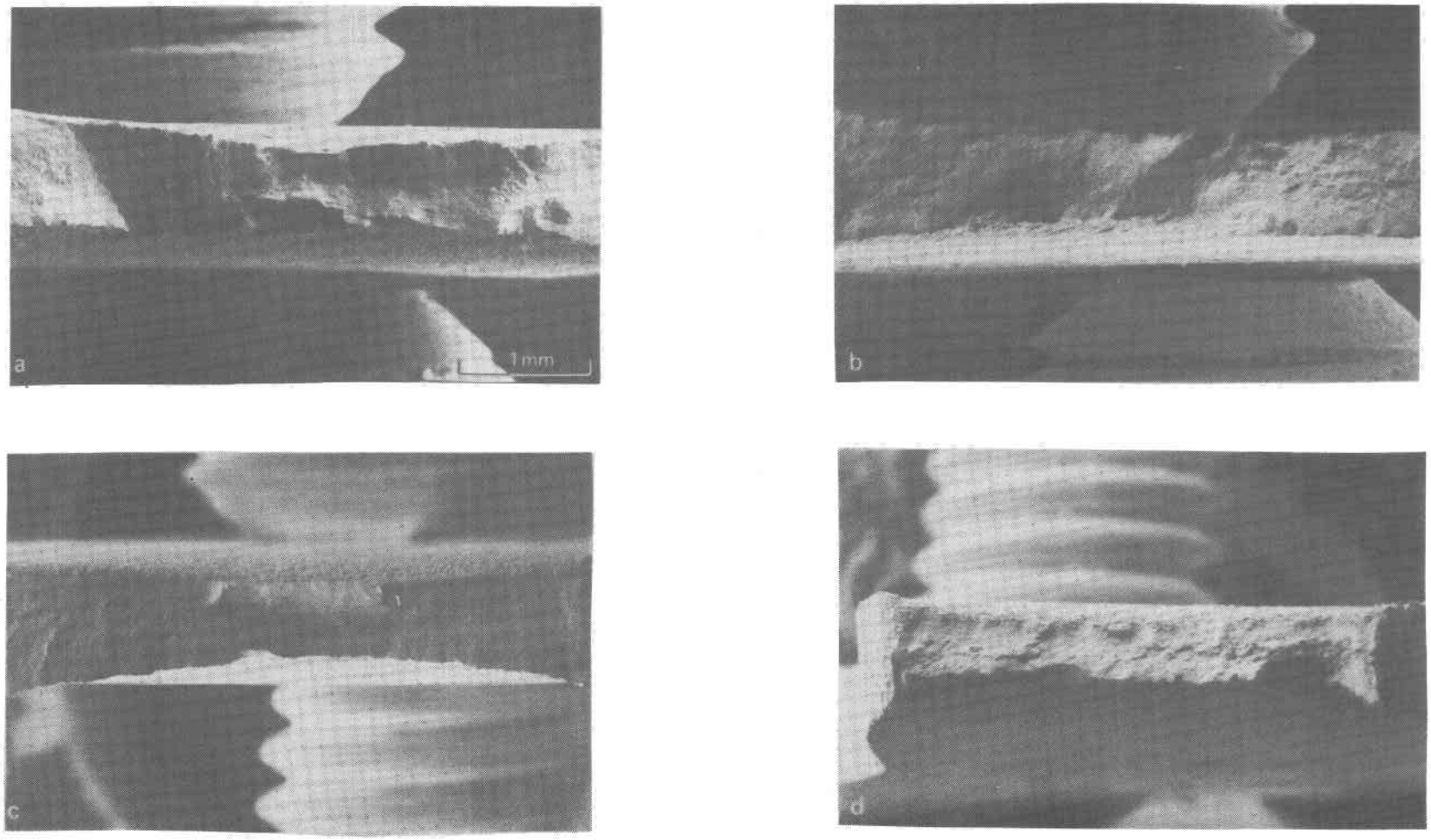

Figure 6. Fracture surfaces for 2.25Cr-1Mo tested at 450°
a) $10^{-5}sec^{-1}$ in salt, b) $10^{-7}sec^{-1}$ in salt,
c) $10^{-5}sec^{-1}$ in air, d) $10^{-7}sec^{-1}$ in air.

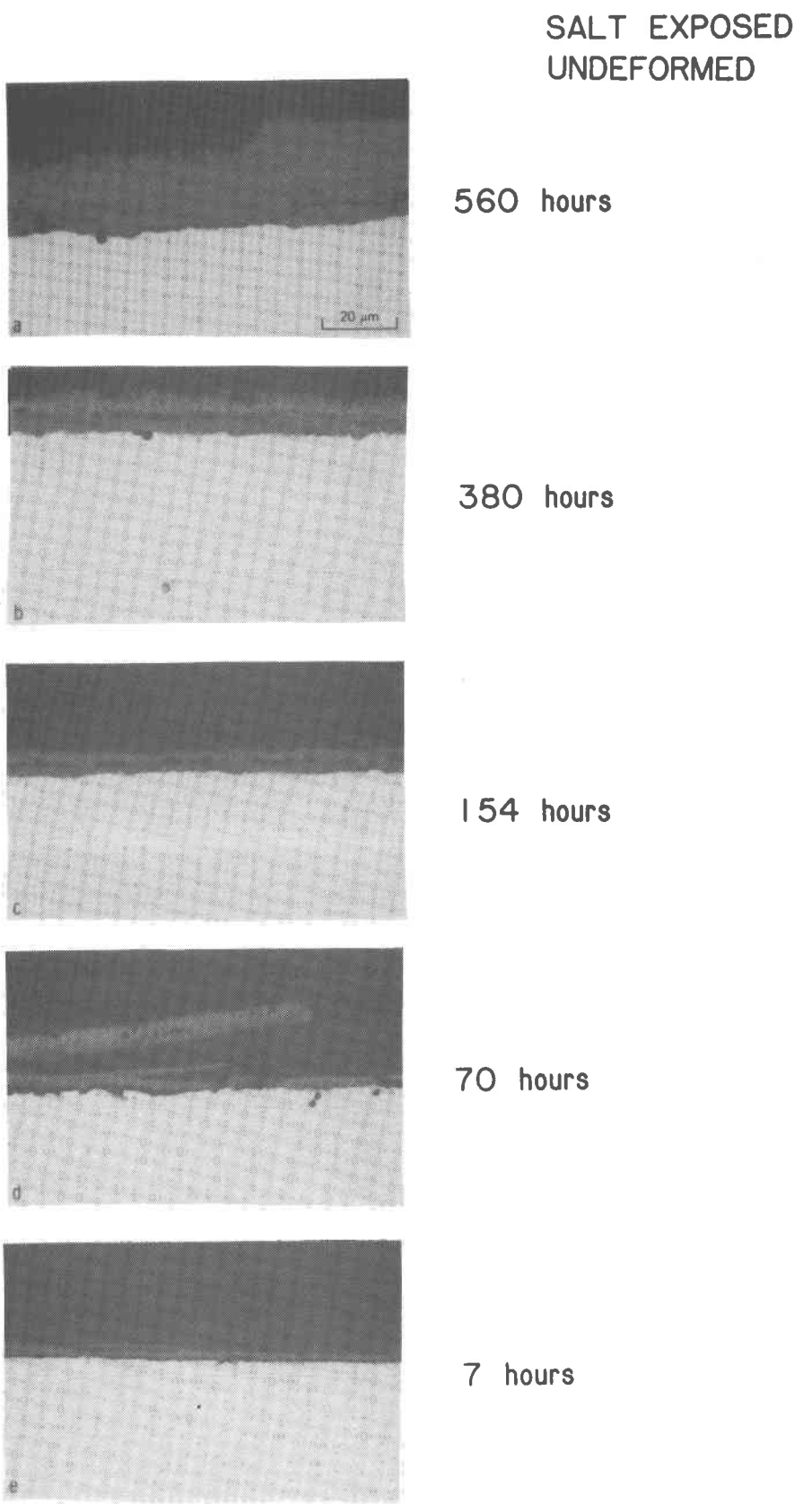

Figure 7. Evolution of surface oxides formed at 450°C on undeformed salt exposed surfaces. Times indicate total test times and therefore approximate the total time at temperature in the environment.

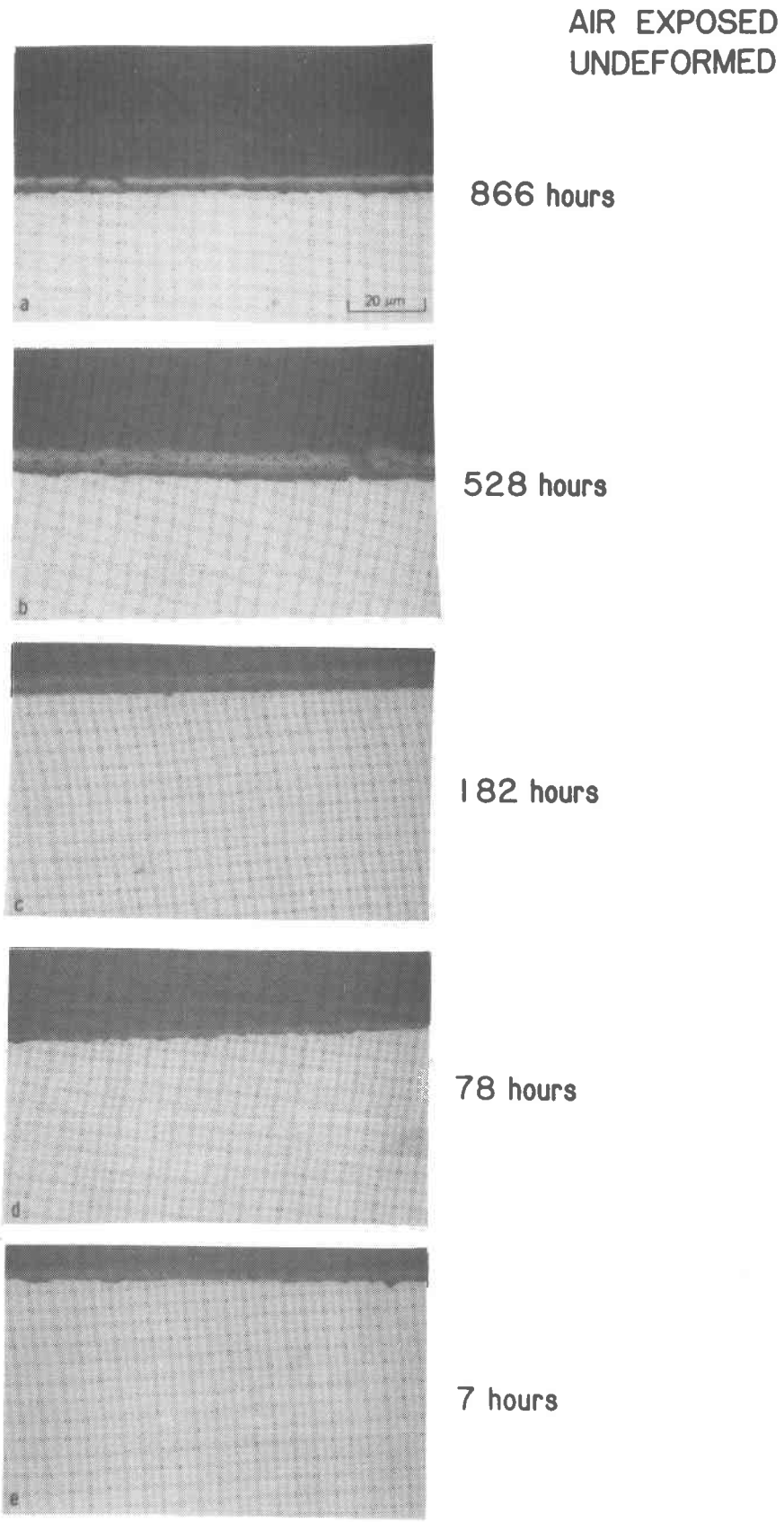

Figure 8. Evolution of surface oxides formed at 450°C on undeformed air exposed surfaces. The times indicate approximate total exposure time at temperature.

Figures 9 and 10 compare the surface scales formed on the salt and air exposed gage surfaces respectively. Again, the times refer to the total test times and therefore approximate the total environmental exposure times. As before, the extent of spallation and oxide cracking is such that quantitative conclusions are not possible. However, the surface scales on the deformed surfaces seem to form more quickly when the alloy is exposed to salt rather than air. In each instance, regardless of strain rate, the oxide layers remaining on the salt exposed surfaces are thicker than those remaining on the air exposed surfaces. Unlike the earlier reported behavior for Alloy 800 (3), deformation of the 2.25Cr-1Mo alloy at 450°C did not seem to measurably increase the rate of scale formation. It is possible, of course, than this observation is influenced by the discussed lack of oxide adherence.

The observed surface oxides tend to be multiphase, as evidenced by the multiple contrast features within the oxides shown in Figures 7-10. EDS analysis revealed that the oxide structure formed in either environment were of similar chemistry, consisting of multiple layers of a chromium-free iron oxide surface scale above a Fe-Cr oxide in which the chromium concentration exceeded that of the base metal. This is illustrated in Figure 11 which indicates that the oxide immediately adjacent to the base metal contained chromium at a level approximately twice that present in the base metal. Molybdenum tends to partition in a like manner as the chromium, being concentrated in the subsurface scale in an amount higher than that present in the base metal.

Mechanical Properties - 525°C

Figure 12 shows the stress strain curves for the alloy tested in air at 525°C and at the same initial strain rates as for the specimens tested at 450°C. At the higher temperature, the ultimate tensile strength of the alloy is more dependent on the initial strain rate that it is at the lower temperature. Increasing the strain rate by two orders of magnitude resulted in an increase of the UTS by approximately 100 MPa. As with the findings at 450°C, the engineering fracture strain tends to decrease with increasing strain rate.

Figure 13 shows the stress strain curves generated for the alloy tested in salt at 525°C and at the same strain rates as at 450°C. The UTS of these specimens exhibited nearly the same strain rate dependence as for the air exposed specimen, increasing by nearly 100 MPa as the strain rate was increased by two orders of magnitude. As for the specimens tested at 450°C, at 525°C the specimens exposed to salt exhibited a higher UTS than those exposed to air. An example of this is shown in Figure 14a which compares the stress-strain curves for salt and air exposed specimens tested at an initial strain rate of $1 \times 10^{-7} sec^{-1}$.

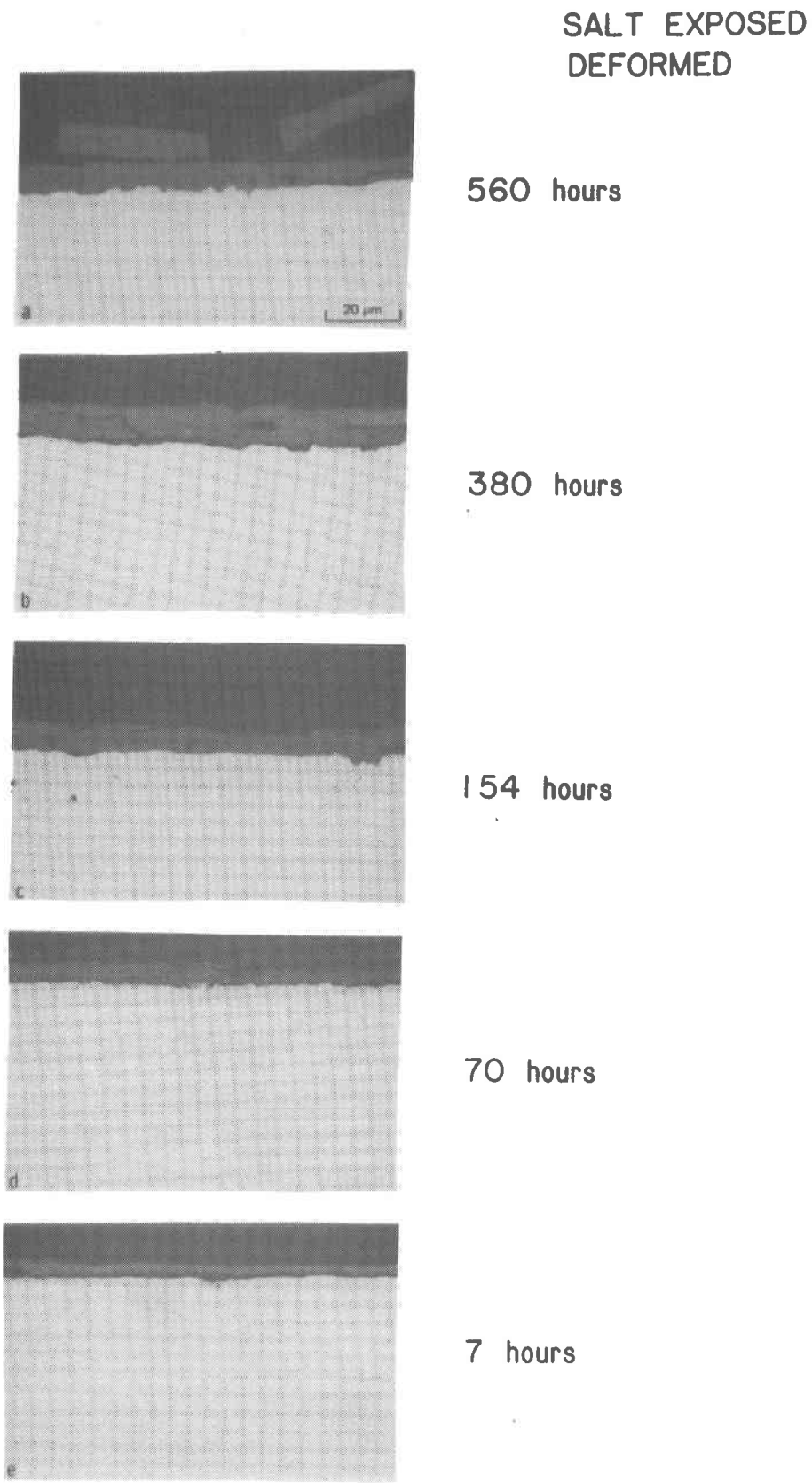

Figure 9. Evolution of surface oxides formed at 450°C on salt exposed deformed gage surfaces.

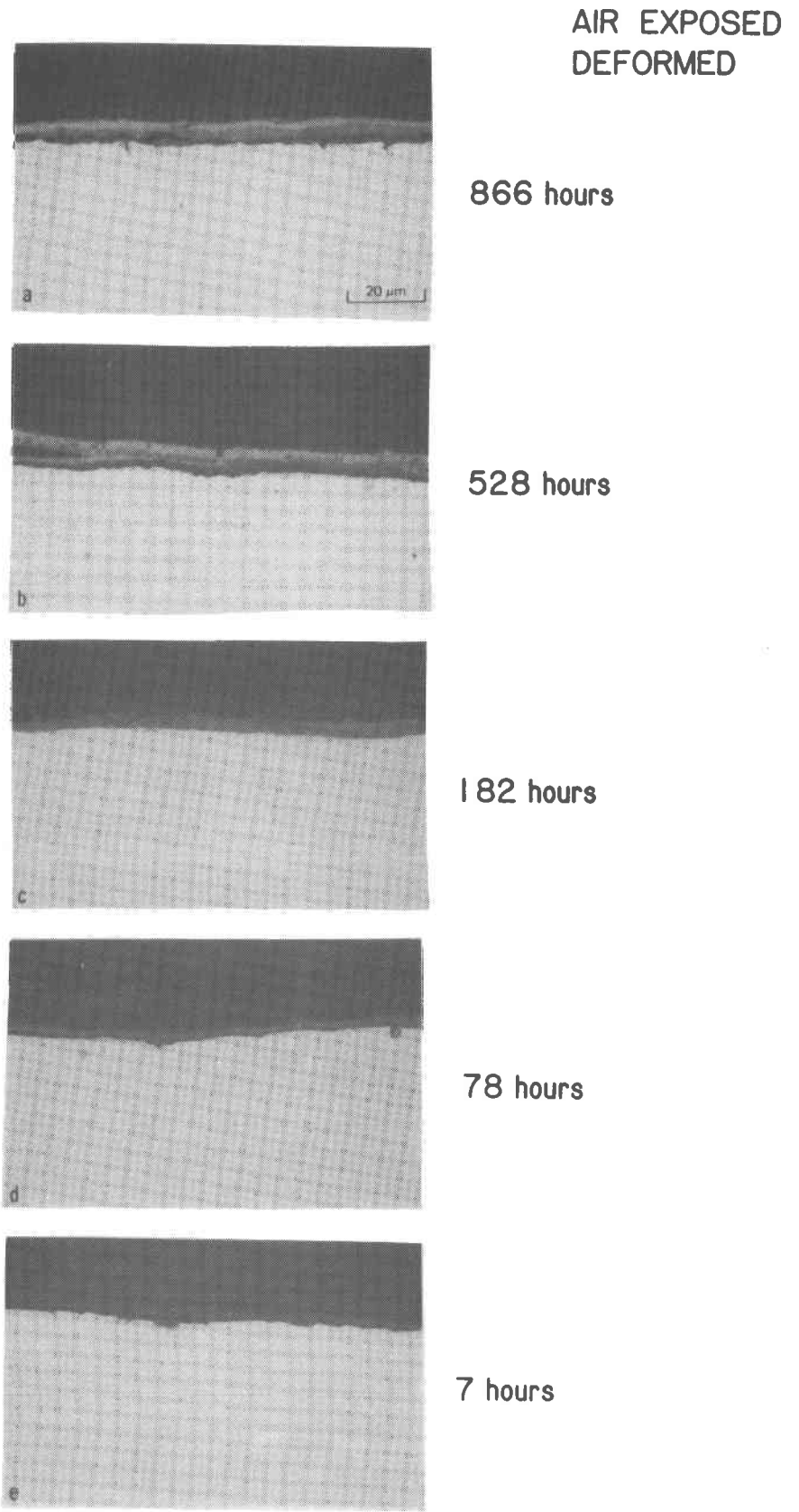

Figure 10. Evolution of surface oxides formed at 450°C on air exposed deformed gage surfaces.

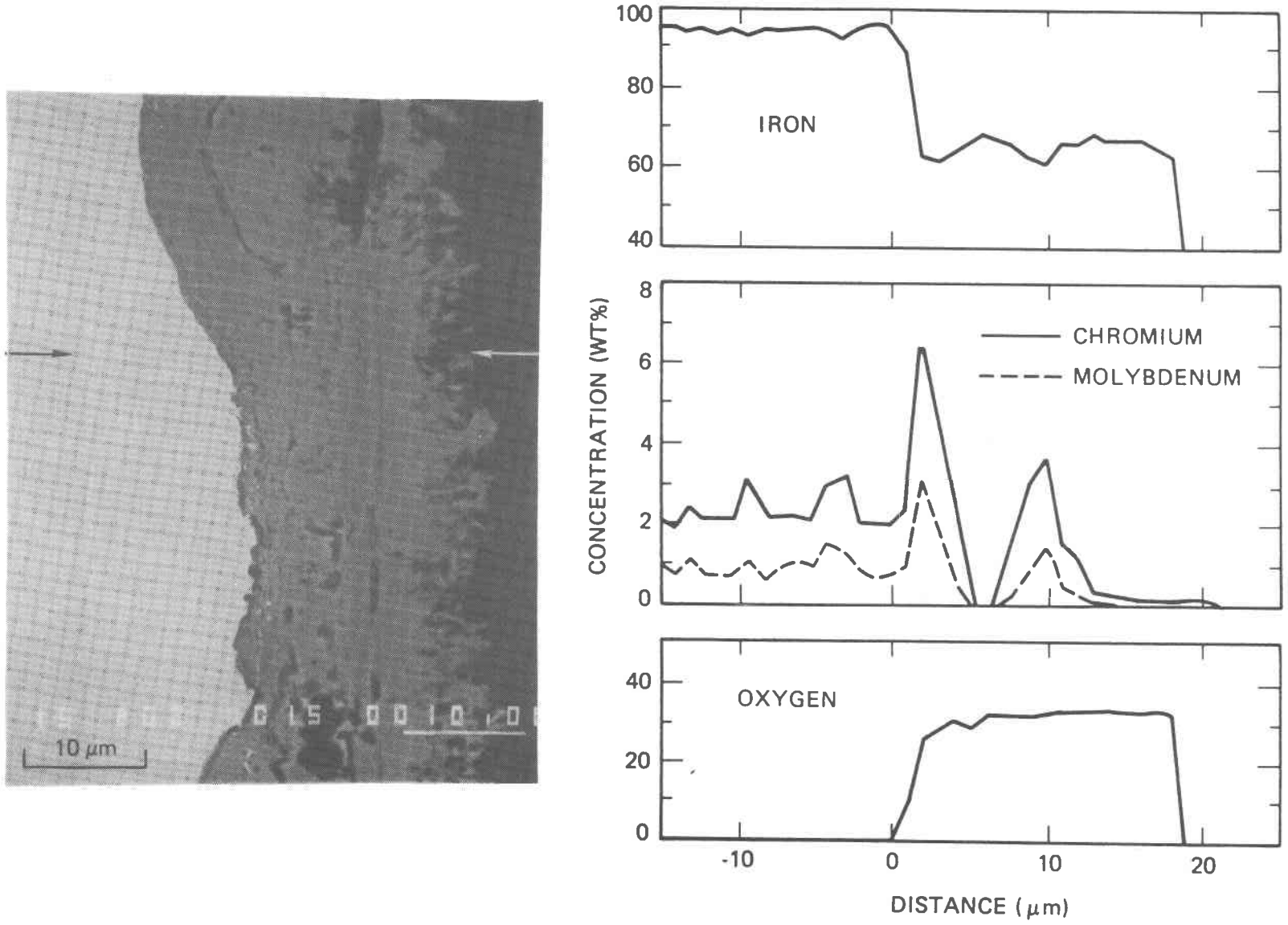

Figure 11. EDS analysis of surface scale formed by contact of 2.25Cr-1Mo to molten nitrate salt for 866 hours at 450°C. Analysis has been performed along the trace defined by the arrows in the micrograph.

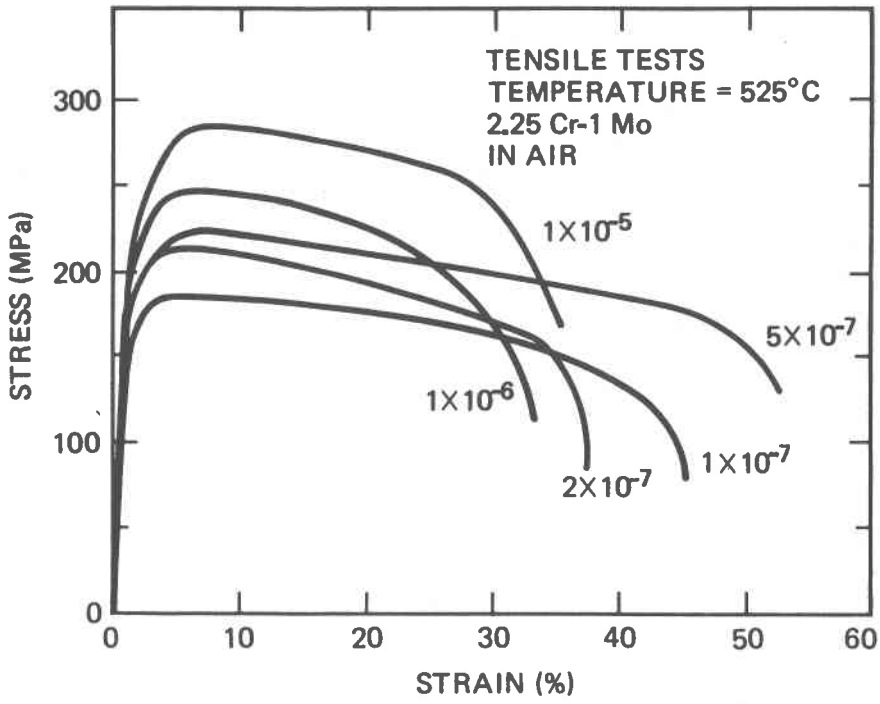

Figure 12. Stress-strain curves for 2.25Cr-1Mo tested in air at 525°C. Strain-rates indicated are in sec^{-1}.

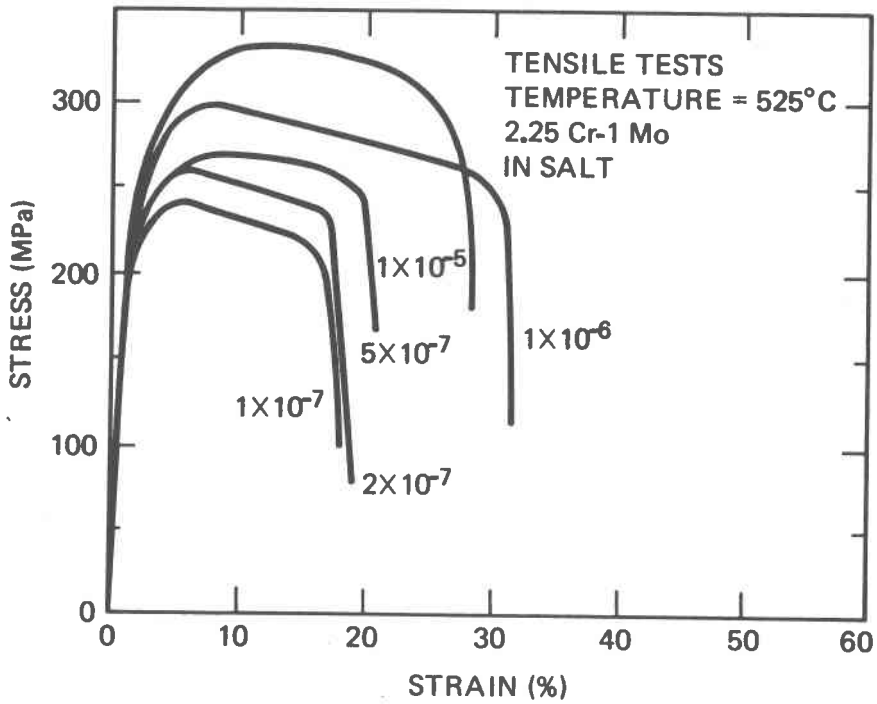

Figure 13. Stress-strain curves for 2.25Cr-1Mo tested in molten salt at 525°C. Strain rates are in sec^{-1}.

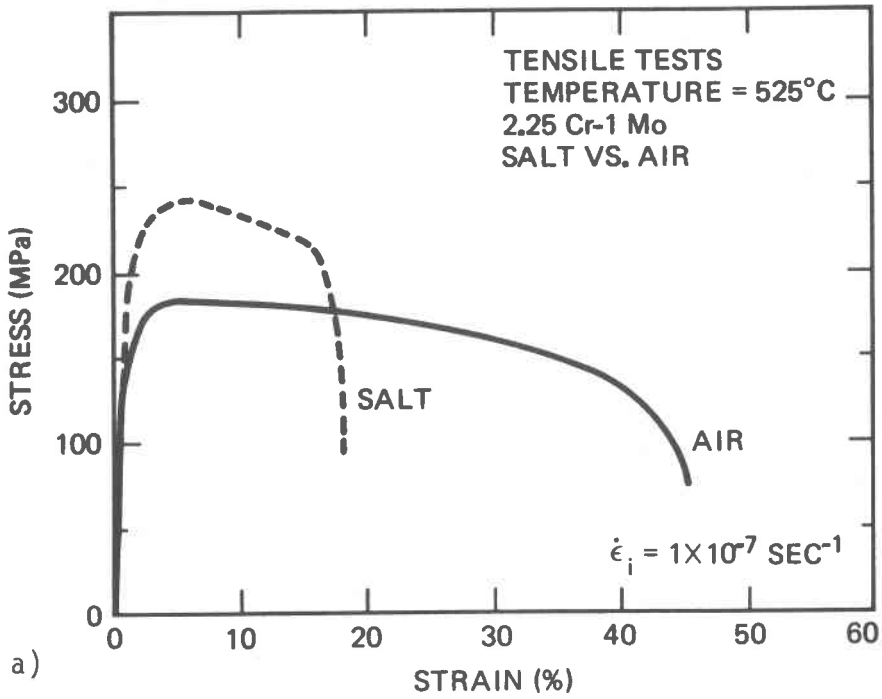

a)

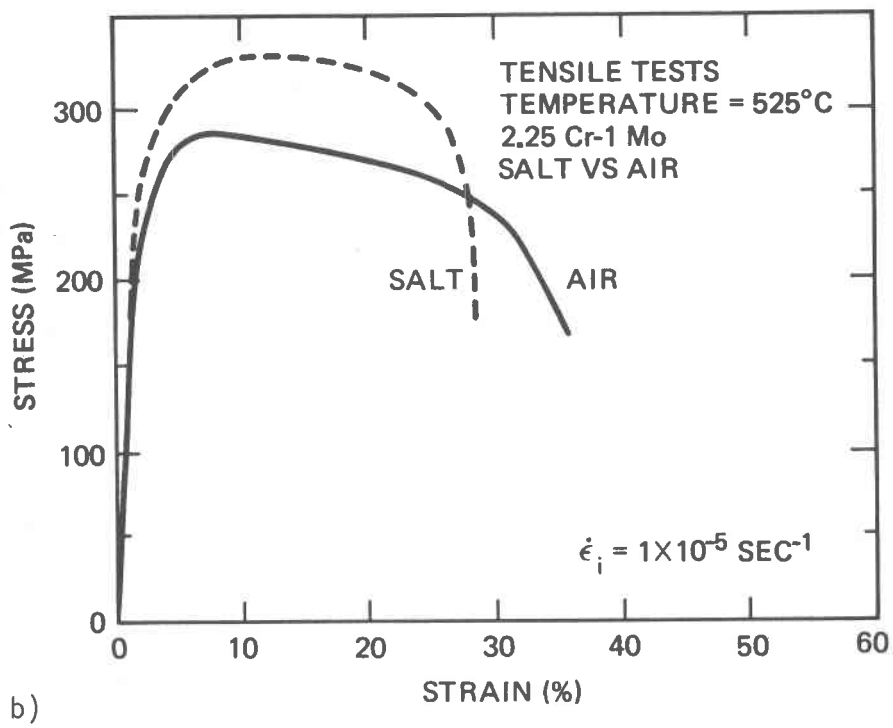

b)

Figure 14. a) Comparison of the tensile behavior of the alloy in salt vs. air at 525°C ($\dot{\varepsilon} = 1 \times 10^{-7}\text{sec}^{-1}$).

b) Comparison of the tensile behavior of the alloy in salt vs. air at 525°C ($\dot{\varepsilon} = 1 \times 10^{-5}\text{sec}^{-1}$).

It is again difficult to rationalize this strengthening in terms of internal oxidation or environmentally induced precipitation of corrosion products, because metallographic observations indicate that the environmental interaction that occurs is purely one of surface attack. The surface scales which form are porous, spall easily, and appear to have very little strength. Thus, it seems unlikely that these surface oxides can be responsible for the observed strengthening. In addition, if the surface scales were responsible for the observed strengthening, the degree of strengthening should be greatest for those specimens tested at the lowest strain rates when the total salt exposure time was longest. Figure 14b reveals that the strengthening increment for specimens tested at $1 \times 10^{-5} sec^{-1}$ was comparable to the increment observed in Figure 14a for specimens tested at the slowest rate. This strengthening by the salt was ubiquitous, occurring at all strain rates examined. Appendix Figure A[2] compares the salt vs. air tensile curves for tests conducted at all other strain rates at this temperature.

The data for all mechanical testing is summarized in Table 3. It can be seen that decreasing the strain rate (increasing salt exposure

TABLE 3

Tensile Properties of 2.25Cr-1Mo at 525°C

Strain Rate (sec^{-1})	Environment	UTS (MPa)	Elongation (%)	RA (%)
1×10^{-5}	Air	283	36.0	82.2
	Salt	329	28.4	44.3
1×10^{-6}	Air	246	34.1	84.3
	Salt	291	31.6	38.6
5×10^{-7}	Air	222	54.3	81.3
	Salt	267	21.0	40.2
2×10^{-7}	Air	214	37.9	78.6
	Salt	256	20.2	41.4
1×10^{-7}	Air	184	46.2	80.0
	Salt	239	18.3	38.6

time) results in a decrease in the ductility of the salt exposed specimens compared to the air exposed specimens. Figures 14a and 14b illustrate this ductility loss as measured by the engineering fracture strain. The effect of environment and strain rate on ductility is summarized in Figure 15. As with the lower temperature results,

reduction in area seems to be a more sensitive measure of environmental effect. At the higher strain rates (10^{-5}, 10^{-6} sec^{-1}), the total elongation was essentially unaffected by the environment while the R.A. measured for the salt exposed specimens was always lower than that measured for specimens tested in air.

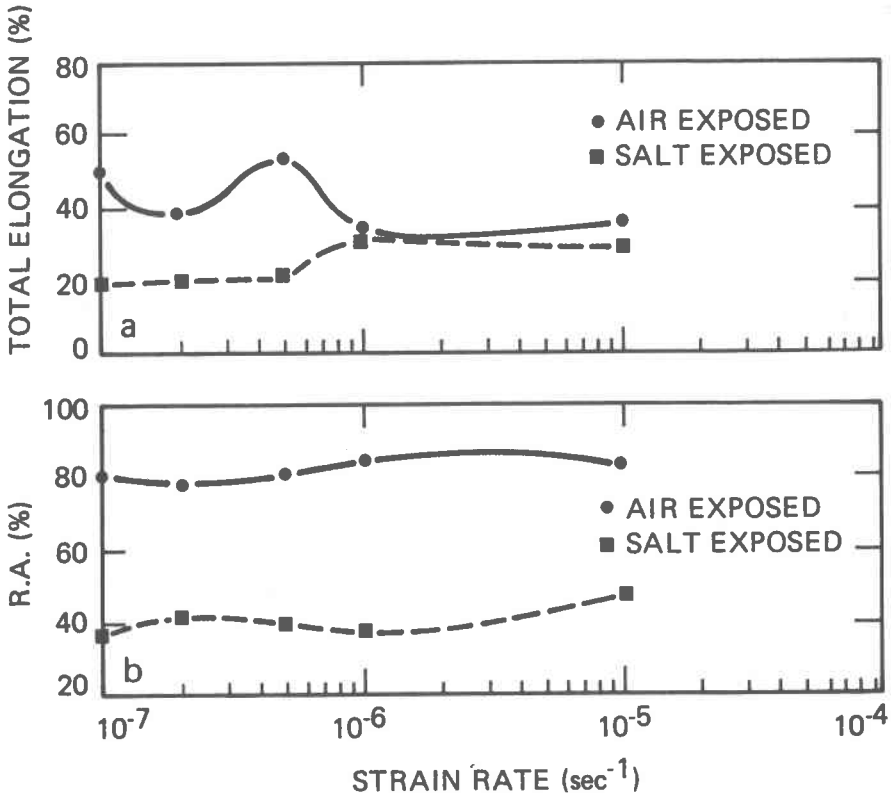

Figure 15. a) Effect of strain rate on total elongation (fracture strain) for 2.25Cr-1Mo at 525°C.

b) Effect of strain rate on reduction in area (R.A.) at 525°C.

Oxide Structure - 525°C

Metallographic observations revealed that the alloy oxidized in both air and salt at this temperature as it did at 450°C. Likewise, the surface scales were generally non-adherent. The extensive spallation which occurred during post-test handling of the specimens again precluded any quantitative measure of the oxidation kinetics or the rate of scale formation. Figure 16 and 17 compare the residual surface scales observed on undeformed grip sections of specimens tested in salt and air, respectively. As in Figures 7 and 8, the times associated with each micrograph represent total test times and therefore approximate the total environmental exposure times at temperature. The surface scales increased in thickness with increasing exposure times. The scales formed during salt exposure were generally thicker than those formed on specimens exposed to air. In many cases there was evidence of

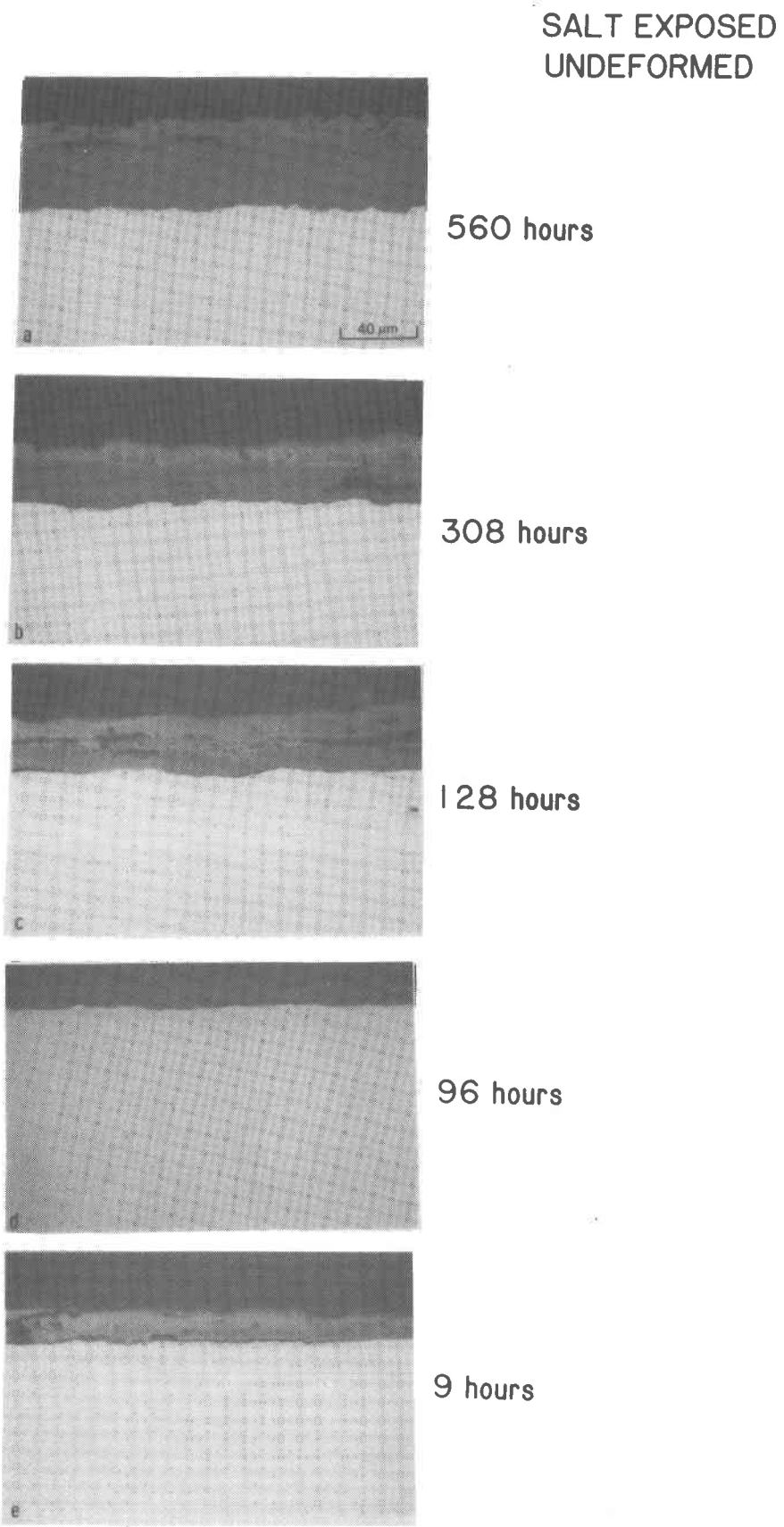

Figure 16. Evolution of surface oxides formed at 525°C on undeformed salt exposed surfaces. Times indicate total test time and therefore approximate the total time at temperature in the environment.

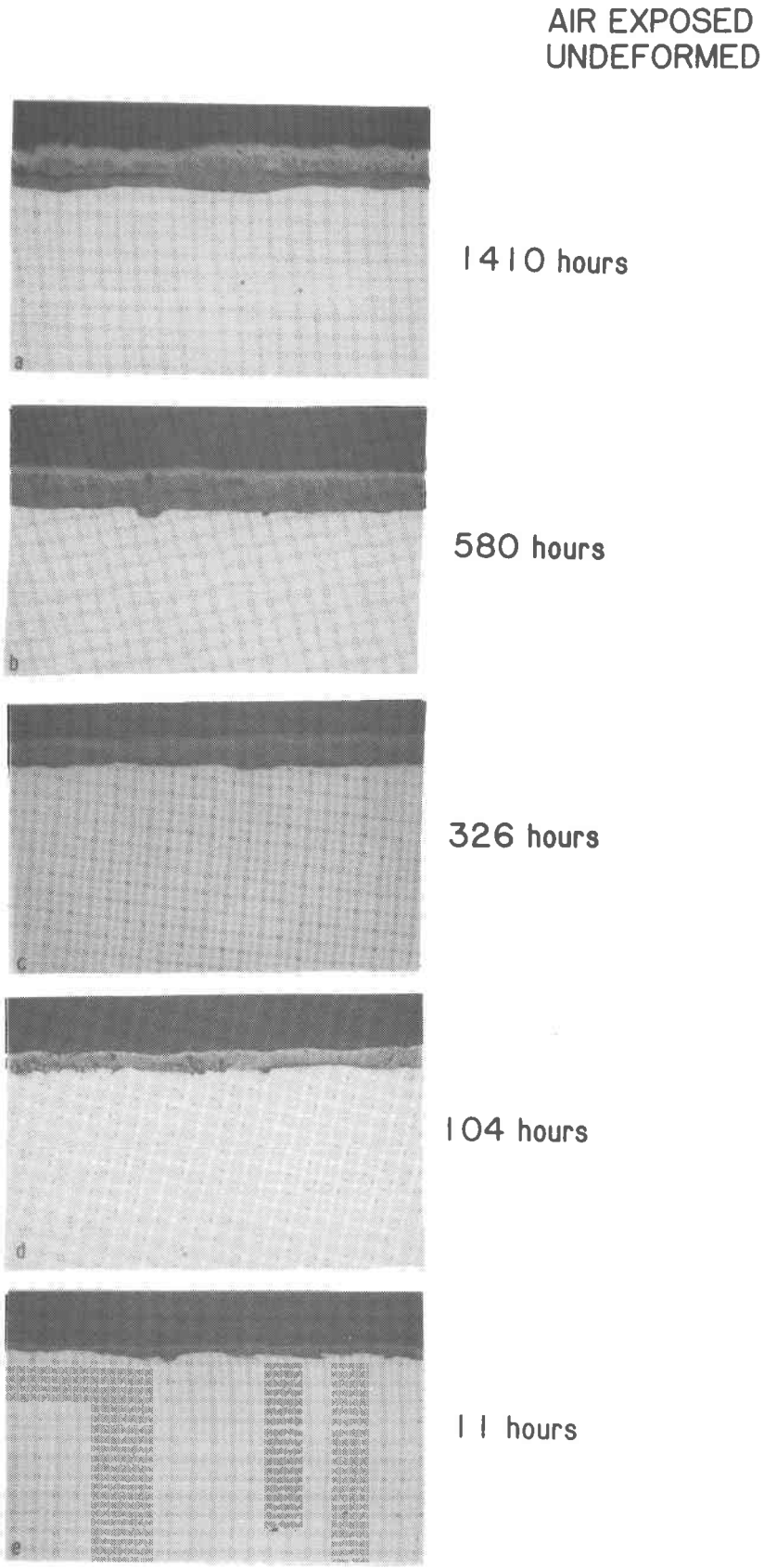

Figure 17. Evolution of surface oxides formed at 525°C on undeformed air exposed surfaces. The times indicate approximate total exposure times at temperature.

extensive oxide cracking and blistering (Fig. 16c). The surface scales which form have a complex structure as indicated by the multiple contrast features visible in the micrographs. These different phase regions are often separated by bands of porosity. It is likely that the observed spallation is the result of the condensation of this porosity.

Figures 18 and 19 compare the surface scales which form on deformed gage sections of salt and air exposed specimens at 525°C. Once again, longer exposure times result in the formation of thicker oxides in both environments. By comparing Figures 16 and 18 or 17 and 19 it can be seen that at this temperature, deformation results in the formation of thicker surface scales for comparable exposure times. For the salt exposed specimens it can also be seen that deformation results in an increased degree of porosity located at the interphase oxide boundary.

Figure 20 shows an EDS analysis of the oxides formed by exposure of the alloy to the molten salt for 560 hours at 525°C. As for the scales formed at 450°C, at the higher temperature, the near-surface iron oxides were Cr-free while the oxide formed adjacent to the base metal contained Cr at levels nearly twice that present in the base metal. Similar to the observations at 450°C, molybdenum appeared to co-segregate with the chromium.

As mentioned above, the rate of scale formation increased with deformation of the base metal. In fact, near the fracture surface, where the specimens have necked (and thus where the local surface deformation is extremely high), the residual oxide scales were extremely thick--as shown in Figure 21. The scale appeared as multiple lamellae of different oxide phases. Such lamellar oxide scales have been observed previously in low alloy ferritic steels (6). This oxide morphology and its extremely rapid rate of growth undoubtedly occurred because the intense local deformation produced repeated fracturing of the oxide. The proposed process is shown schematically in Figure 22. Initially, upon contact with the salt environment, the duplex oxide structure forms (Fig 22B). With prolonged exposure the oxide thickens everywhere along the gage surface (Fig. 22C). When deformation becomes locally intense during necking, the oxide fractures, exposing fresh base metal and providing a path for contact with the salt (Fig 22D). A new generation of the dual phase scale then forms as shown in Figure 22E. Because the salt is in direct contact with the base metal, diffusion of the oxidizing species through the original scale is not required and so the corrosion rate is high. Since this process is occurring in a region of intense deformation the evolving surface scale continues to crack frequently. New layers of oxide continue to form (Fig. 22F), rapidly consuming the base metal. Thus, the alloy is most susceptible to environmental degradation once a plastic instability has formed.

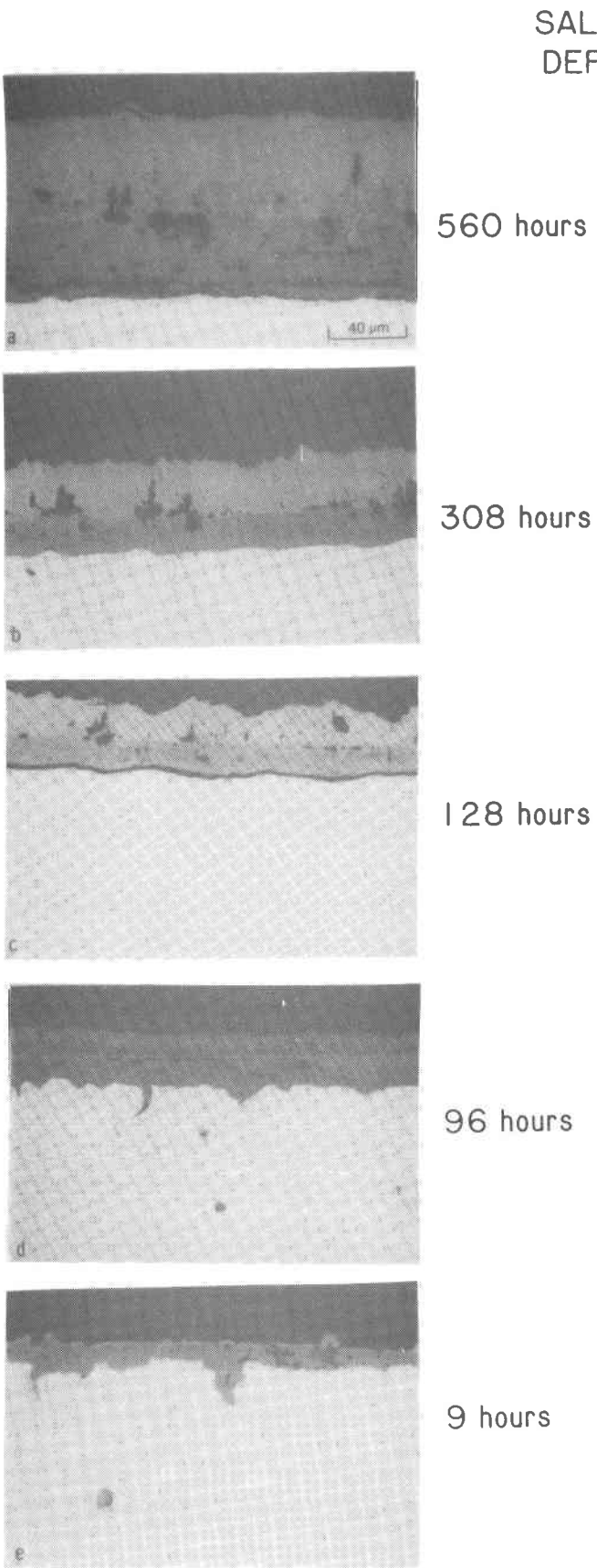

Figure 18. Evolution of surface oxides formed at 525°C on salt exposed deformed gage surfaces.

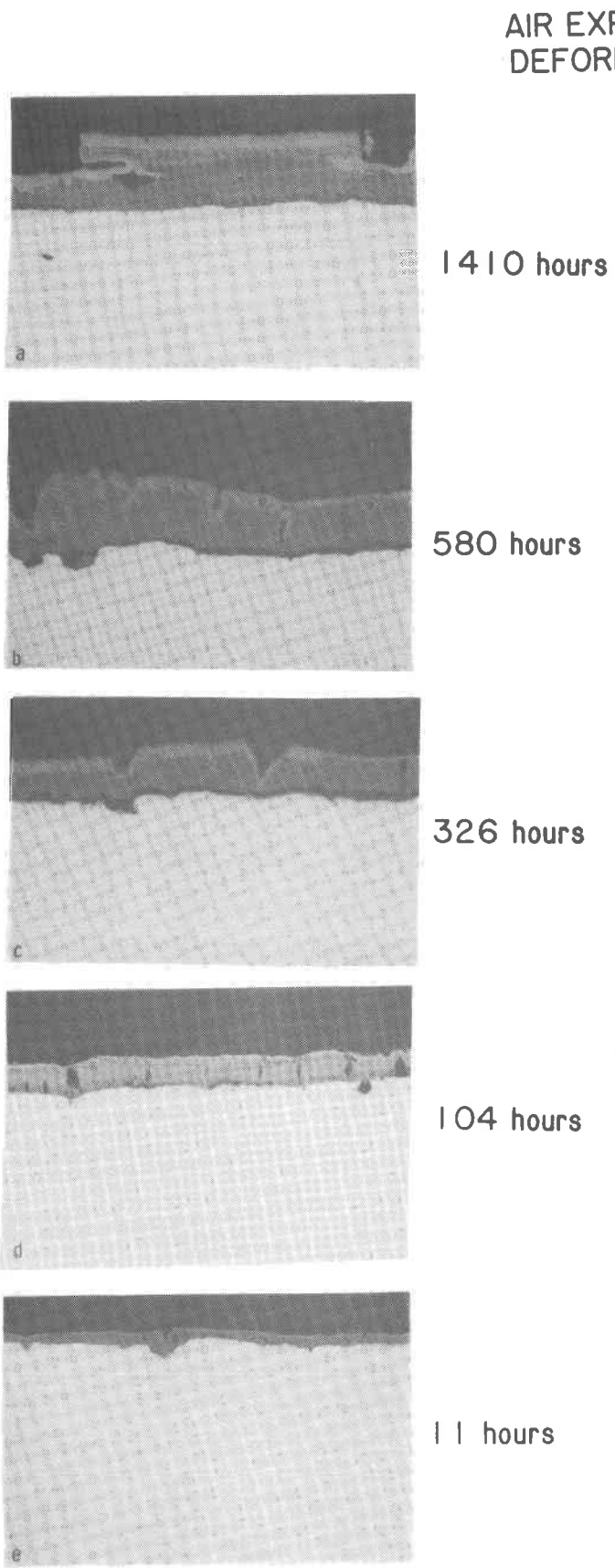

Figure 19. Evolution of surface oxides formed at 525°C on air exposed deformed gage section.

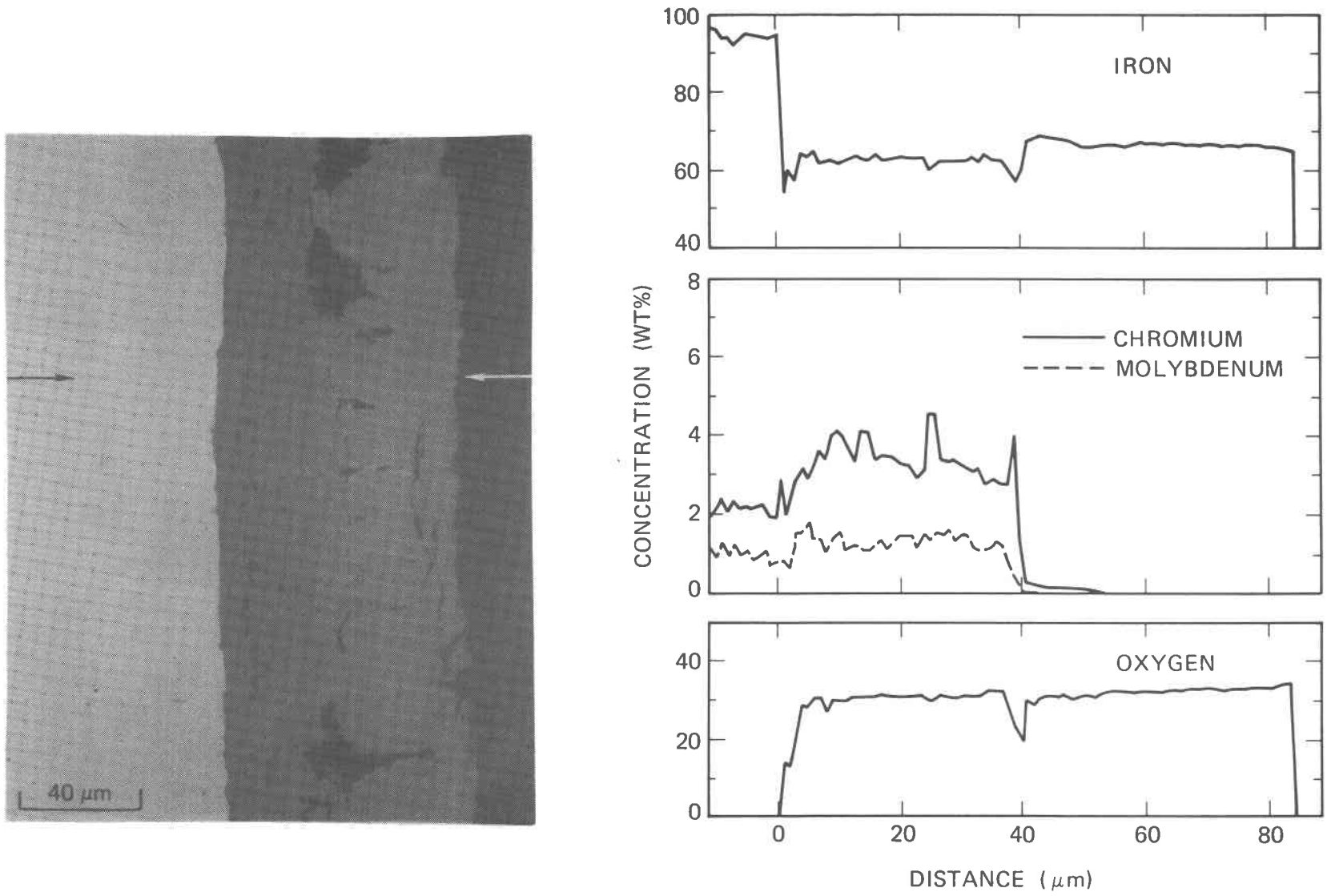

Figure 20. EDS analysis of surface scale formed by contact of 2.25Cr-1Mo to molten nitrate salt at 525°C after 560 hours. Analysis performed along the trace defined by the arrows in the micrograph reveals the oxide to be duplex in structure.

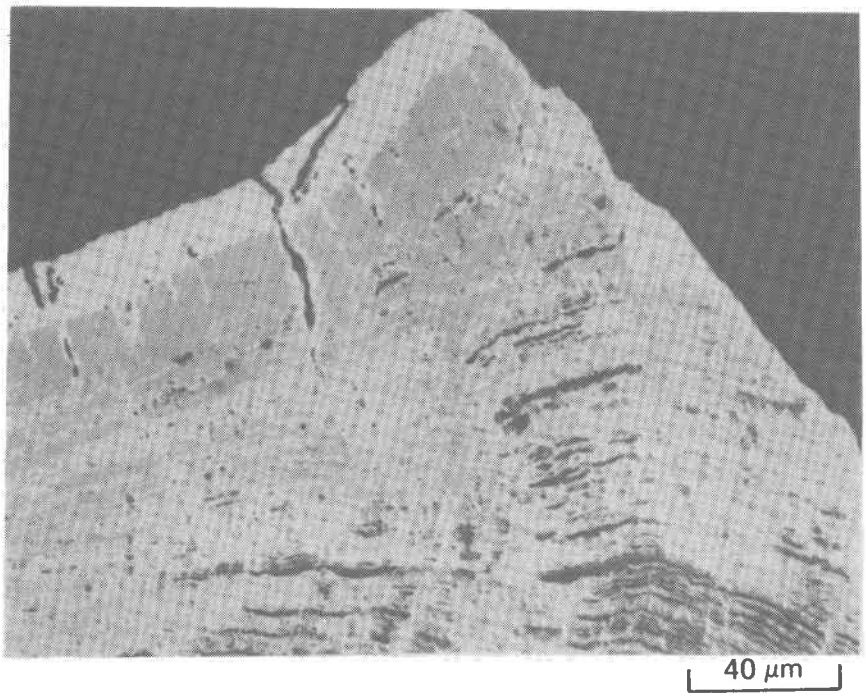

Figure 21. Oxide formed on deformed gage section just below fracture surface. Laminar layers consist of the Fe-rich and Cr-rich oxide phases discussed in the text.

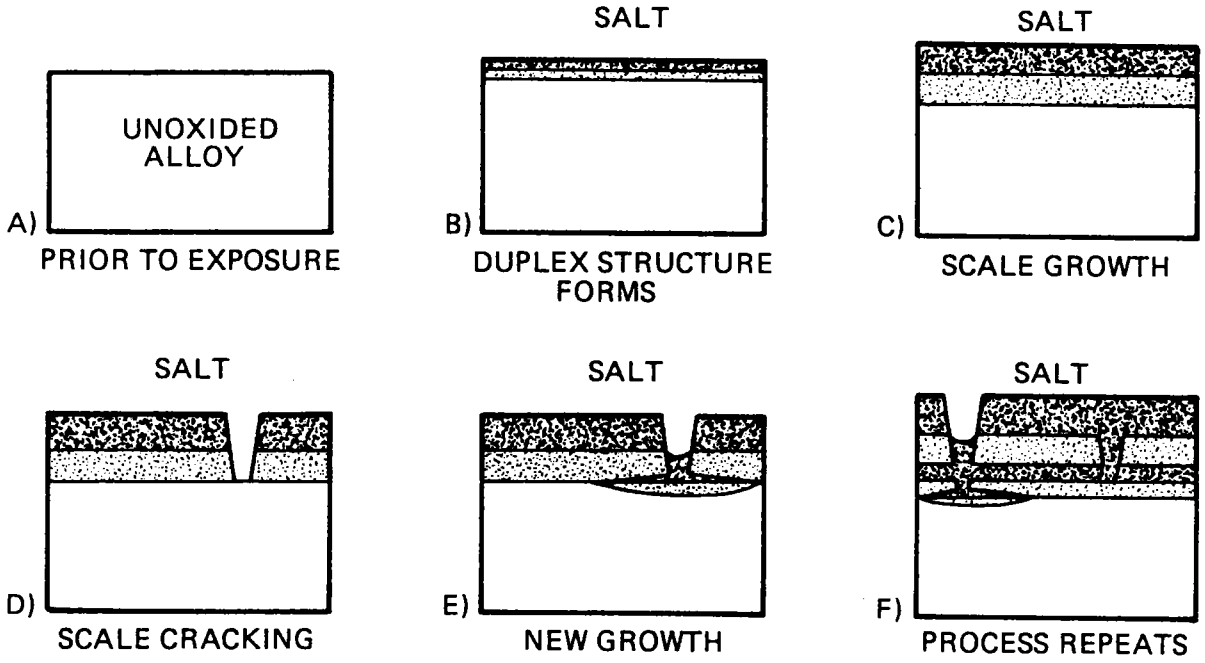

Figure 22. Schematic representation of the process by which the laminar oxides evolve.

Conclusions

The results of the mechanical testing in molten salt have revealed the presence of an environmentally-induced degradation of mechanical properties. Strain to fracture, reduction in area and ultimate tensile strength were appreciably affected by exposure of the alloy to the nitrate salt environment at both 450°C and 525°C. At both temperatures the engineering fracture strain of the salt exposed specimens was less than that of the air exposed specimens for strain rates below $10^{-6}sec^{-1}$, while reduction in area for the salt exposed specimens was below that for the specimens tested in air at all strain rates examined. Contact with the molten salt resulted in increased tensile strength when compared to specimens tested in air at comparable strain rates.

The fragility of the oxide and its lack of adherence precluded any quantitative measure of the rate of oxide formation as a function of time, or of the influence of deformation on the scale growth kinetics. However, the residual oxides observed on surfaces in contact with salt were always thicker than those formed on surfaces in contact with air for comparable lengths of time.

Deformation apparently increases the rate of oxide formation on uniformly deformed surfaces compared to unstrained surfaces, at least at 525°C. Upon necking, the increase in the rate of surface straining results in a dramatic increase in the rate of scale formation which appears as a multiple lamellar structure. This observation can be understood as resulting from repeated strain induced oxide cracking, which exposes unoxidized base metal. Upon contact with the molten salt environment, the base metal then rapidly re-oxidizes. As the base metal is consumed in the necked region due to the increase rate of corrosion, the effective load bearing cross-section is reduced, accelerating the rate of deformation and resulting in the measured overall ductility loss.

Acknowledgements

The assistance of T. J. Sage (8316) for his aid in specimen preparation and in the design and operation of the mechanical testing equipment is gratefully acknowledged.

REFERENCES

1. R. W. Carling and R. W. Mar, Industrial use of Molten Nitrate/Nitrate Salts, Sandia National Labortories, Livermore, SAND81-8020, Dec. 1981.

2. C. M. Kramer, W. H. Smyrl and W. B. Estill, J. Mater. for Energy Systems, Vol. 1, p. 59, 1980.

3. S. H. Goods, J. Mater. for Energy Systems, Vol. 3, p. 43, 1980.

4. R. W. Bradshaw, Corrosion of 304SS by Molten $NaNo_3$-KNO_3 in a Thermal Convection Loop, Sandia National Laboratories, Livermore, SAND80-8856, Dec. 1980.

5. K. H. Dohle, A. Ramel, M. Schmidt, and M. Schultze, Corrosion and Mechanical Stress at High Temperature, Eds. V. Guttmann and M. Merq, Applied Science Pub. London 1981, p. 441.

6. J. E. Forrest and P. S. Bell, Corrosion and Mechanical Stress at High Temperatures, Eds. V. Guttmann and M. Merz, Applied Science Pub., London, 1981, p. 339.

APPENDIX

A[1] Additional comparisons of the tensile behavior of 2.25Cr-1Mo in salt vs. air at 450°C.

A[2] Additional comparisons of the tensile behavior of 2.25Cr-1Mo in salt vs. air at 525°C.

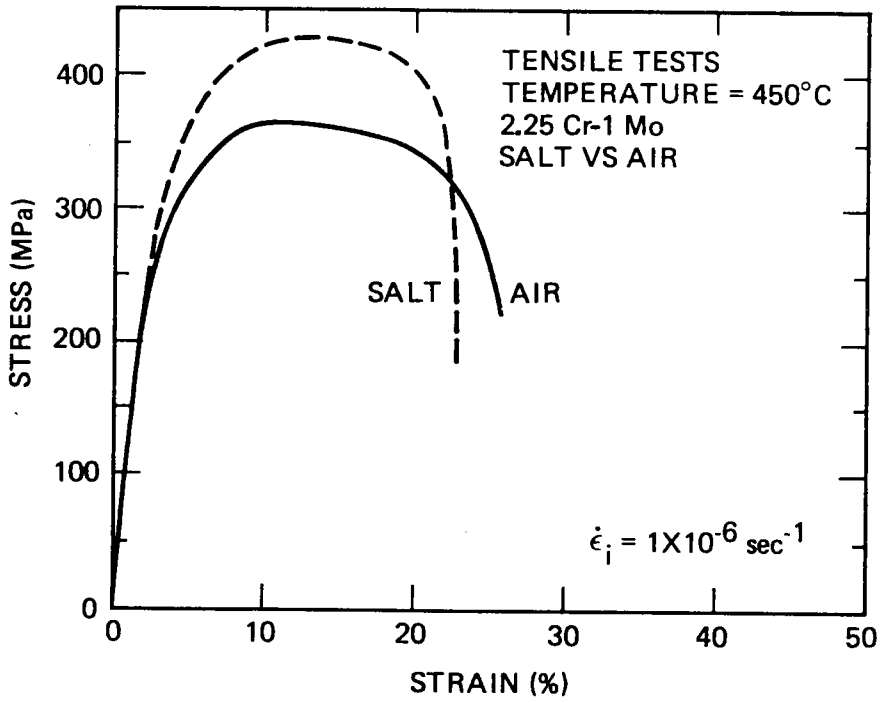
TENSILE TESTS
TEMPERATURE = 450°C
2.25 Cr-1 Mo
SALT VS AIR
SALT
AIR
$\dot{\epsilon}_i = 1X10^{-6}$ sec^{-1}
STRESS (MPa)
STRAIN (%)
0
100
200
300
400
0
10
20
30
40
50

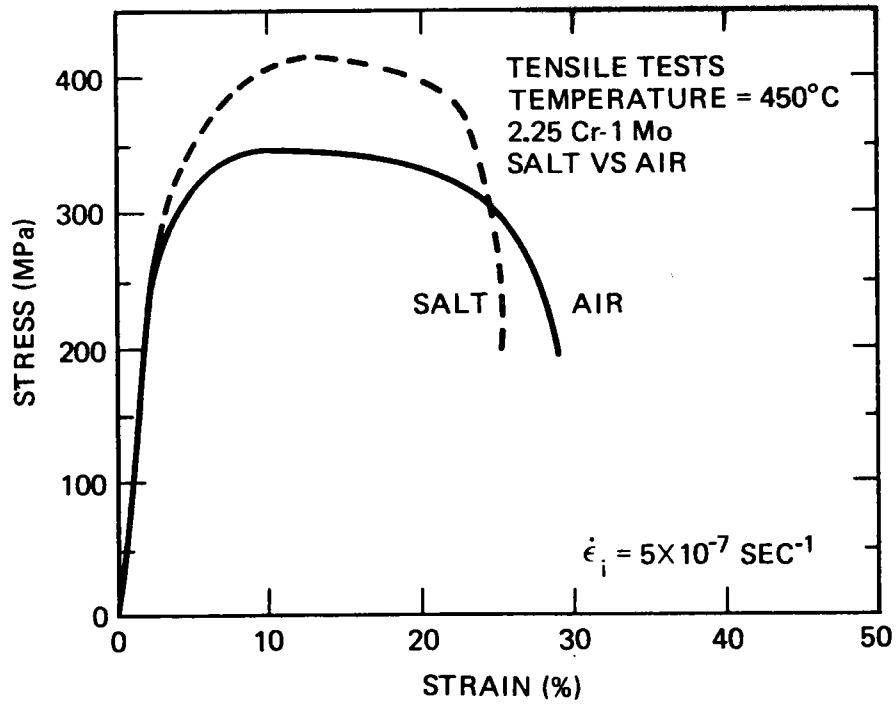
TENSILE TESTS
TEMPERATURE = 450°C
2.25 Cr-1 Mo
SALT VS AIR
SALT
AIR
$\dot{\epsilon}_i = 5X10^{-7}$ SEC^{-1}
STRESS (MPa)
STRAIN (%)
0
100
200
300
400
0
10
20
30
40
50

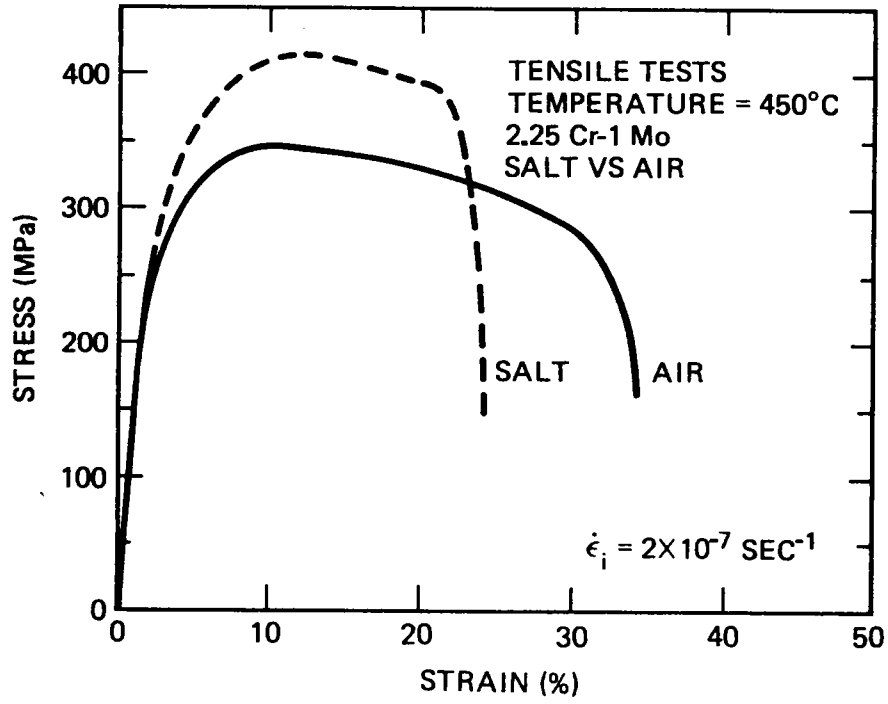
TENSILE TESTS
TEMPERATURE = 450°C
2.25 Cr-1 Mo
SALT VS AIR
SALT
AIR
$\dot{\epsilon}_i = 2X10^{-7}$ SEC^{-1}
STRESS (MPa)
STRAIN (%)
0
100
200
300
400
0
10
20
30
40
50

Figure A[1]

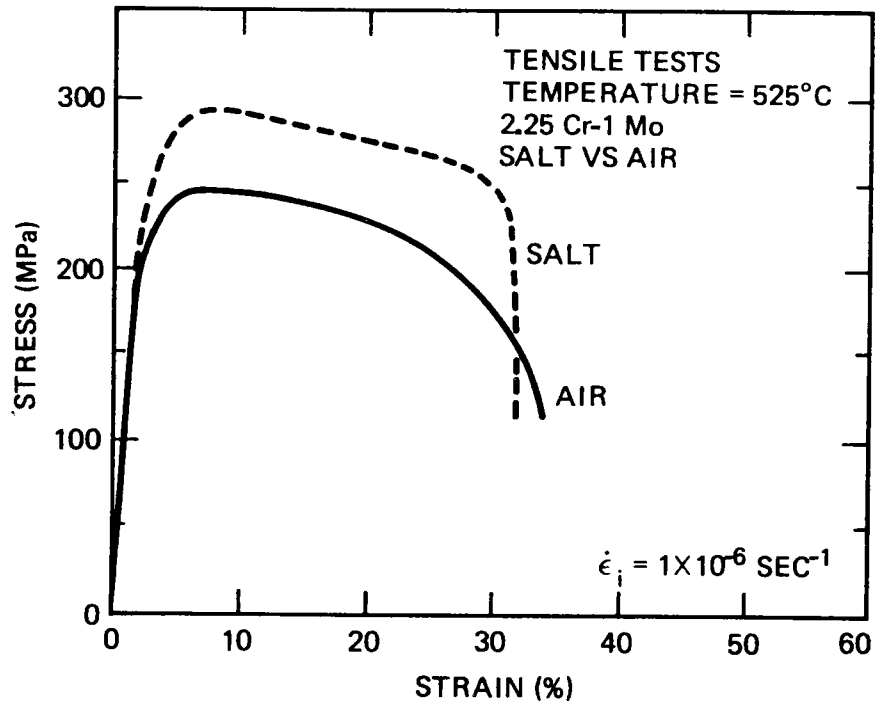
TENSILE TESTS
TEMPERATURE = 525°C
2.25 Cr-1 Mo
SALT VS AIR
SALT
AIR
$\dot{\epsilon}_i = 1X10^{-6}$ SEC^{-1}
STRESS (MPa)
STRAIN (%)
0
100
200
300
0
10
20
30
40
50
60

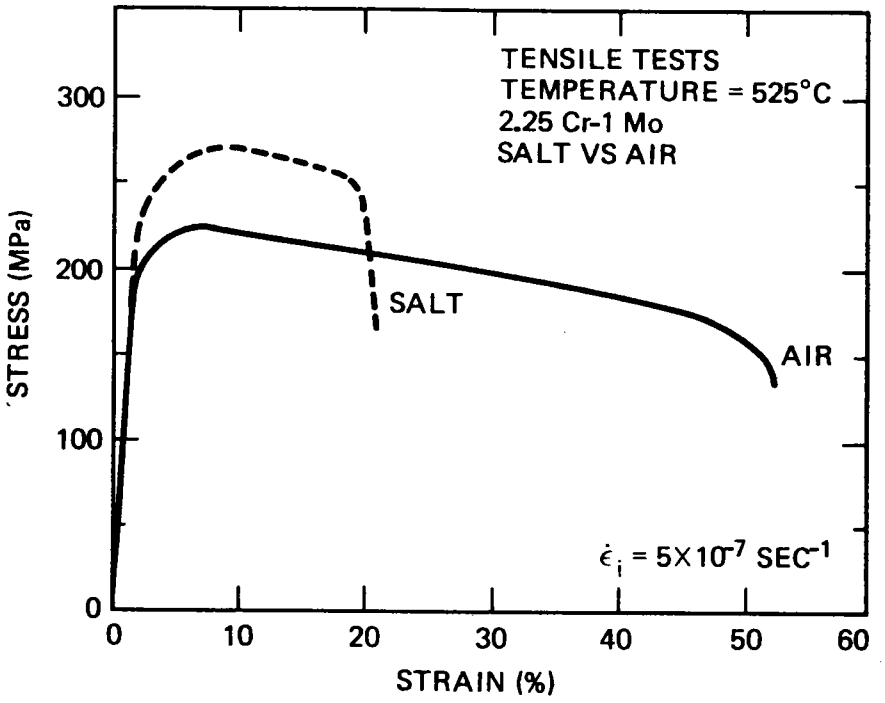
TENSILE TESTS
TEMPERATURE = 525°C
2.25 Cr-1 Mo
SALT VS AIR
SALT
AIR
$\dot{\epsilon}_i = 5X10^{-7}$ SEC^{-1}
STRESS (MPa)
STRAIN (%)
0
100
200
300
0
10
20
30
40
50
60

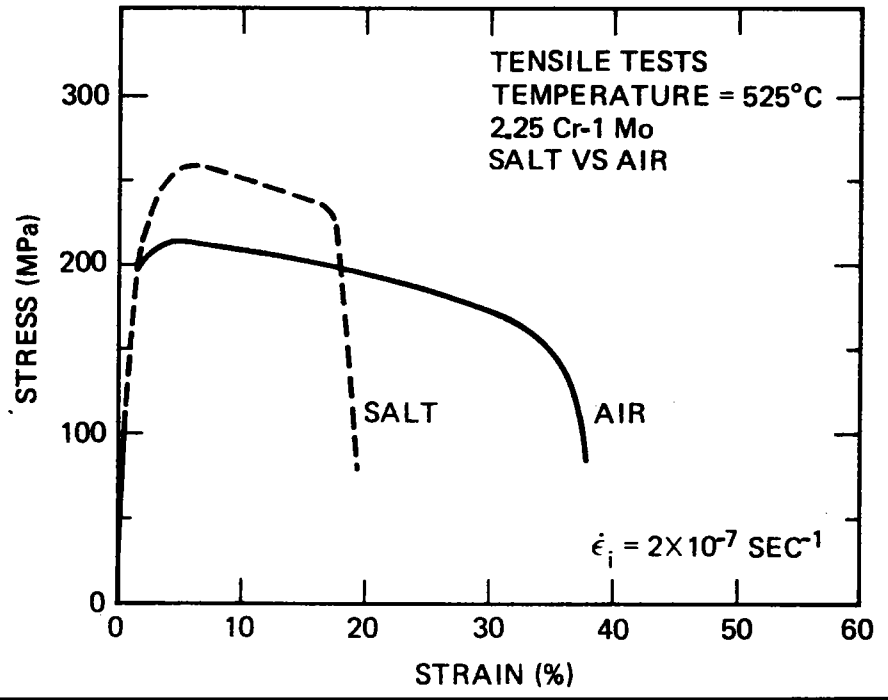
TENSILE TESTS
TEMPERATURE = 525°C
2.25 Cr-1 Mo
SALT VS AIR
SALT
AIR
$\dot{\epsilon}_i = 2X10^{-7}$ SEC^{-1}
STRESS (MPa)
STRAIN (%)
0
100
200
300
0
10
20
30
40
50
60

Figure A [2]

UNLIMITED RELEASE

INITIAL DISTRIBUTION

U. S. Department of Energy (3)
Division of Solar Thermal Technology
James Forrestal Building
1000 Independence Avenue, S.W.
Washington, D.C. 20585
Attn: G. W. Braun
M. Scheve
C. B. McFarland

U. S. Department of Energy
Division of Thermal and Chemical Energy Storage Systems
James Forrestal Building
1000 Independence Avenue, S.W.
Washington, D.C. 20585
Attn: J. H. Swisher

U. S. Department of Energy
San Francisco Operations Office
Division of Solar Technology
1333 Broadway
Oakland, CA 94612
Attn: R. W. Hughey

Arizona Public Service Co.
P.O. Box 21666
Phoenix, AZ 85036
Attn: E. Weber

Babcock & Wilcox
20 S. Van Buren Avenue
Barberton, OH 44203
Attn: G. Grant

Babcock & Wilcox
Research and Development Division
1562 Beeson Street
Alliance, OH 44601
Attn: P. Daniel

Badger Energy, Inc.
One Broadway
Cambridge, MA 02142
Attn: C. A. Bolthrunis

Bechtel Corporation (2)
P. O. Box 3965
San Francisco, CA 94119
Attn: E. Lam
R. Lessley

Black & Veatch Consulting Engineers (2)
P.O. Box 8405
Kansas City, MO 64114
Attn: J. E. Harder
J. C. Grosskreutz

Combustion Engineering, Inc.
1000 Prospect Hill Road
Windsor, CN 06095
Attn: G. H. Rowe

EIC Laboratories, Inc.
55 Chapel Street
Newton, MA 02158
Attn: S. H. White

EG&G Idaho, Inc.
P.O. Box 1625
Bldg. ARA-I
Idaho Falls, ID 83415
Attn: R. Neilson, Jr.

Electric Power Research Institute
P.O. Box 10412
3412 Hillview Avenue
Palo Alto, CA 94303
Attn: E. DeMeo

Energy Concepts Co.
627 Ridgely
Annapolis, MD 21401
Attn: D. C. Ericksen

Foster Wheeler Development Corporation (3)
12 Peach Tree Hill Road
Livingston, NJ 07039
Attn: R. J. Zoschak
A. C. Gangadharan
W. R. Apblett

Gas Cooled Reactor Association
3344 N. Torrey Pines Road
La Jolla, CA 92137
Attn: D. J. Spellman

General Atomic Company (2)
P.O. Box 81608
San Diego, CA 92138
Attn: T. H. VanHagen
J. L. Kaae

Jet Propulsion Laboratory
4800 Oak Grove Drive
Pasadena, CA 91103
Attn: V. Truscello

Martin Marietta Corporation (2)
P.O. Box 179
Denver, CO 80201
Attn: T. R. Tracey
R. K. McMordie

McDonnell Douglas Astronautics Company (5)
5301 Bolsa Avenue
Huntington Beach, CA 92647
Attn: R. Easten
D. L. Endicott
L. Dreier
C. M. Finch
R.Riedesal

Oak Ridge National Laboratory
P.O. Box X
Oak Ridge, TN 37830
Attn: J. H. DeVan

Olin Corporation (2)
275 Winchester Avenue
New Haven, CT 06511
Attn: L. C. Fiorucci
S. L. Goldstein

Olin Corporation (2)
120 Long Ridge Road
Stamford, CT 06904
Attn: N. Christopher
R. E. Smith

Dr. Robert A. Osteryoung
Department of Chemistry
State University of New York at Buffalo
Buffalo, NY 14214

Pacific Gas and Electric Company (2)
Department of Engineering Research
3400 Crow Canyon Road
San Ramon, CA 94583
Attn: H. E. Seielstad
J. Raggio

Park Chemical Company
8074 Military Avenue
Detroit, MI 48204
Attn: R. W. Foreman

Public Service Company of New Mexico
P.O. Box 2267
Albuquerque, NM 87103
Attn: D. J. Groves

Rockwell International
Energy Systems Group
8900 De Soto Avenue
Canoga Park, CA 91304
Attn: T. Springer

Rockwell International (2)
Rocketdyne Division
6633 Canoga Avenue
Canoga Park, CA 91304
Attn: J. M. Friefeld
W. T. Chandler

Sierra Pacific Power Company
P.O. Box 10100
Reno, NV 89501
Attn: R. G. Richards

Solar Energy Research Institute (3)
1617 Cole Boulevard
Golden, CO 80401
Attn: B. Butler
B. P. Gupta
SERI Library

Southern California Edison (2)
P.O. Box 800
Rosemead, CA 91770
Attn: J. N. Reeves
R. S. Williamson

Southwestern Public Service Company
P.O. Box 1261
Amarillo, TX 79170
Attn: K. Ladd

Solar Thermal Systems
Division of Exxon Enterprises, Inc.
P.O. Box 592
Florham Park, NJ 07932

Stearns-Roger Engineering Corporation
P.O. Box 58888
Denver, CO 80217
Attn: W. R. Lang

West Texas Utilities Company
P. O. Box 841
Abilene, TX 79604
Attn:: R. R. Stanaland

R. L. Schwoebel, 1800; Attn: M. J. Davis, 1830
K. E. Mead, 1811
N. J. Magnani, 1840
R. B. Diegel, 1841
E. H. Beckner, 9700; Attn: D. G. Schueler, 9720
R. S. Claassen, 8000; Attn: D. M. Olson, 8100
A. N. Blackwell, 8200
L. Gutierrez, 8400
D. L. Hartley, 8500
B. F. Murphey, 8300; Attn: R. L. Rinne, 8320
G. W. Anderson, 8330
W. Bauer, 8340
R. W. Rohde, 8310
D. A. Nissen, 8312
D. K. Ottesen, 8313
R. W. Bradshaw, 8313
A. S. Nagelberg, 8313
M. W. Perra, 8314
L. A. West, 8315
J. C. Swearengen, 8316
S. H. Goods, 8316 (5)
J. B. Wright, 8450
A. C. Skinrood, 8452
W. G. Wilson, 8453
J. Woodard, 8454
D. B. Dawson, 8454
Publications Division, 8265, for TIC (2)
Publications Division, 8264/Technical Processes Division, 3141
Technical Library Processes Division, 3141 (3)
M. A. Pound, 8214 for Central Technical Files (3)

Org.	Bldg.	Name	Rec'd by	Org.	Bldg.	Name	Rec'd by

Sandia National Laboratories